Neuroscience Research xxx (2010) xxx–xxx

Contents lists available at ScienceDirect

Neuroscience Research

journal homepage: www.elsevier.com/locate/neures

Cerebral activation associated with speech sound discrimination during the diotic listening task: An fMRI study

Yumiko Ikeda[a], Noriaki Yahata[a,1], Hidehiko Takahashi[b], Michihiko Koeda[c], Kunihiko Asai[d], Yoshiro Okubo[c], Hidenori Suzuki[a,*]

[a] Department of Pharmacology, Nippon Medical School, 1-1-5, Sendagi, Bunkyo-ku, Tokyo 113-8602, Japan
[b] Department of Molecular Neuroimaging, Molecular Imaging Center, National Institute of Radiological Sciences, 4-9-1, Anagawa, Inage-ku, Chiba 263-8555, Japan
[c] Department of Neuropsychiatry, Nippon Medical School, 1-1-5, Sendagi, Bunkyo-ku, Tokyo 113-8602, Japan
[d] Asai Hospital, 38-1, Katoku, Togane, Chiba 283-0062, Japan

ARTICLE INFO

Article history:
Received 22 July 2009
Received in revised form 4 February 2010
Accepted 5 February 2010

Keywords:
Auditory attention
Diotic listening
Functional MRI
Left anterior superior temporal gyrus
Left inferior temporal gyrus
Right superior temporal gyrus

ABSTRACT

Comprehending conversation in a crowd requires appropriate orienting and sustainment of auditory attention to and discrimination of the target speaker. While a multitude of cognitive functions such as voice perception and language processing work in concert to subserve this ability, it is still unclear which cognitive components critically determine successful discrimination of speech sounds under constantly changing auditory conditions. To investigate this, we present a functional magnetic resonance imaging (fMRI) study of changes in cerebral activities associated with varying challenge levels of speech discrimination. Subjects participated in a diotic listening paradigm that presented them with two news stories read simultaneously but independently by a target speaker and a distracting speaker of incongruent or congruent sex. We found that the voice of distracter of congruent rather than incongruent sex made the listening more challenging, resulting in enhanced activities mainly in the left temporal and frontal gyri. Further, the activities at the left inferior, left anterior superior and right superior loci in the temporal gyrus were shown to be significantly correlated with accuracy of the discrimination performance. The present results suggest that the subregions of bilateral temporal gyri play a key role in the successful discrimination of speech under constantly changing auditory conditions as encountered in daily life.

1. Introduction

Selective listening is an auditory process that enables one to attend to a specific speech of interest among a mixture of parallel conversations. Accomplishment of this ability, commonly known as the cocktail party effect, requires not only appropriate orientation and sustainment of auditory attention but also a multitude of concomitant cognitive processes including sound discrimination, human voice recognition, language processing, and so forth. To reveal the underlying neural mechanisms, the so-called dichotic listening paradigm has long been used as an effective measure in combination with neuroimaging studies (Pugh et al., 1996; Beaman et al., 2007). In this paradigm, two different auditory stimuli are presented simultaneously, but with one of the stimuli delivered to one ear and the second to the other ear (Kimura, 1961; Bryden, 1988). The types of auditory stimuli ranged from simple tones (Jäncke et al., 2003; Petkov et al., 2004) to syllables (Lipschutz et al., 2002), to meaningful words (Grady et al., 1997; Jäncke et al., 2001), and to sentences (Hashimoto et al., 2000). Previous imaging studies based on this paradigm and using positron emission tomography (PET) and functional magnetic resonance imaging (fMRI) have revealed brain regions implicated in selective listening. Robust activity is observed in the bilateral temporal lobes, including the superior temporal gyrus (STG) (Tzourio et al., 1997; Alho et al., 1999; Hugdahl et al., 1999; Zatorre et al., 1999; Hashimoto et al., 2000; Jäncke et al., 2001; van den Noort et al., 2008) during dichotic listening tasks. These areas are well known to be involved in auditory perception (van den Noort et al., 2008). In addition, significant activation is found in the lateral frontal (Hashimoto et al., 2000; Lipschutz et al., 2002; Thomsen et al., 2004) and parietal cortices (Hashimoto et al., 2000; Lipschutz et al., 2002; van den Noort et al., 2008). Mid-ventrolateral (BA 45/47) and mid-dorsolateral areas (BA 9/46) in the lateral frontal cortex are involved in pruning out unwanted information by responding selectively to relevant information (Lipschutz et al., 2002). The parietal cortex, especially the temporoparietal junction extending toward the inferior parietal lobe (IPL), plays a major role in attentional orientation during dichotic listening (Lipschutz et al., 2002). Therefore,

* Corresponding author. Tel.: +81 3 3822 2131; fax: +81 3 5814 1684.
E-mail address: hsuzuki@nms.ac.jp (H. Suzuki).
[1] Present address: Department of Neuropsychiatry, Graduate School of Medicine, University of Tokyo, 7-3-1, Hongo, Bunkyo-ku, Tokyo 113-8655, Japan.

0168-0102/$ – see front matter © 2010 Elsevier Ireland Ltd and the Japan Neuroscience Society. All rights reserved.
doi:10.1016/j.neures.2010.02.006

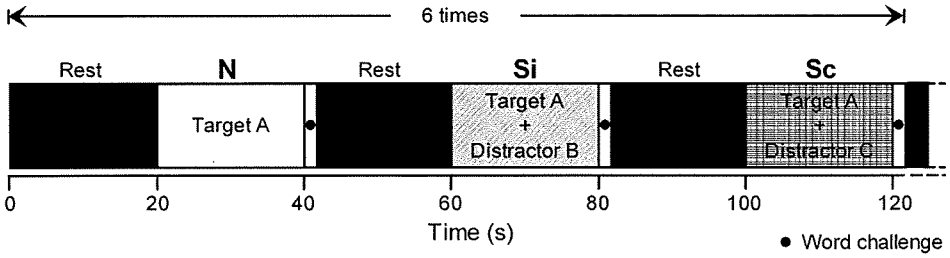

Fig. 1. The experimental block design of the session. Three conditions were sequentially presented to subjects: N, non-selective listening, a news story read out by a target speaker only; Si, selective listening, news stories read out by a target speaker and a distracting speaker of incongruent sex; Sc, selective listening, news stories read out by a target speaker and a distracting speaker of congruent sex. Each condition was presented for 20 s and interleaved with 20-s rest. After each condition, a word was displayed on a screen for 2 s (black circle) for the subjects to answer whether or not it was present in the target news of the preceding block by pressing a button. Each session was repeated six times.

the dichotic listening paradigm has a major advantage in specifying brain areas involved in the selective listening process, although speech discrimination under the constantly changing auditory conditions as encountered in daily life is far from such dichotic listening settings.

While the dichotic listening paradigm is one extreme abstraction of selective listening processes that we encounter in daily life, another experimental paradigm, the diotic listening paradigm, has also been used in previous studies, albeit less frequently, to investigate auditory attention under more natural listening settings. The task consists of binaural presentation of target stimuli superimposed by distracting stimuli (Scott et al., 2004; Shafiro and Gygi, 2007), so that the listening condition is more compatible with that in our daily life where the speech of interest and other conversations are typically mixed together and delivered to both ears. Previously, an fMRI study based on this paradigm reported that discrimination of human speech is associated with blood oxygenation level-dependent (BOLD) activation in Wernicke's area (BA22), Broca's area (BA44/45) and the frontal association cortex (BA6, 9/46, 32, 13/47), suggesting that the neural networks for executing semantic, syntactic, and prosodic processing are implicated in speech discrimination (Nakai et al., 2005). Given that constantly changing auditory environments are encountered in daily life, it is still unclear which brain regions critically work in response to change of challenge level in speech sound discrimination paradigms.

Here we present an fMRI study based on the diotic listening paradigm to evaluate brain activity involved in auditory selective attention. We found that hemodynamic activities in some temporal subregions showed significant correlations with performance accuracy of speech sound discrimination.

2. Materials and methods

2.1. Subjects

Twenty healthy volunteers, 10 males and 10 females, participated in the study (mean age ± SD, 24.9 ± 2.0 years). All subjects were right-handed according to the Edinburgh handedness inventory (mean laterality quotients ± SD, 89.7 ± 15.7) (Oldfield, 1971) and were native speakers of Japanese with normal hearing. None had a previous history of any neurological or psychiatric disorders. All subjects gave written informed consent prior to participation in the experiment. The present study was approved by the Ethics Committees of Nippon Medical School and Asai hospital.

2.2. Experimental design

The diotic listening task consisted of three conditions: (1) a reference condition wherein a single news story was read out by a target speaker (N condition), (2) a diotic listening condition wherein two distinct news stories were read out simultaneously but independently by the target and another speaker (distracter) of incongruent sex (Si condition), and (3) the same as Si condition except the sex of the distracter was congruent (Sc condition). Compared to the Si condition, the congruency of the sex of the speaker in the Sc condition was expected to make speech discrimination more challenging, since male and female reportedly have different phonation frequencies in reading possibly due to anatomical differences in vocal folds (Chen, 2007). The expected different levels of difficulty in speech sound discrimination were defined as 'challenge level' hereafter. The news stories were adopted from television programs and segmented into a 20-s long clip by a digital sound editor (Ulead MediaStudio Pro 6.0, Ulead Systems, Torrance, CA, USA). Each news segment contained 2.5 ± 2.3 sentences in each condition, which were read at a rate of 8.6 ± 0.6 characters/s.

A block design was used for the presentation of stimuli during the fMRI session. An active block of 20-s duration, corresponding to one of three listening conditions, was interleaved with resting periods of the same duration (Fig. 1). The order of conditions was fixed to N–Si–Sc, and this sequence was repeated six times in a single session (i.e., six news stories per condition). The target voice remained identical within a single sequence of conditions (N–Si–Sc), so the subjects could identify during the N condition which voice they should have attended to in the subsequent diotic listening conditions (Si and Sc). To avoid habituation to a particular voice, however, the target voices were altered across the sequences.

To quantify the degree of comprehension of stories read by the target voices, a word challenge was employed at each end of the block. A single word was visually presented for 2 s immediately after each block, and the subjects were required to judge if the word was present or absent in the preceding news segment.

The task presentation during the scan was controlled by SuperLab Pro 2.0.4 (Cedrus Corporation, San Pedro, CA, USA). Auditory stimuli were delivered binaurally through headphones (Resonance Technology Inc., Northridge, CA, USA). Visual stimuli were delivered to a translucent mirror attached to a head coil by a projector located outside the scanner room. During the scan, the subjects were instructed to use their index finger when answering the word challenge.

2.3. fMRI data acquisition

Functional imaging data were acquired with a 1.5 Tesla Signa system with a standard head coil (General Electric, Milwaukee, WI). Functional images of 180 volumes were acquired from each subject with T2*-weighted gradient-echo echo-planar imaging sequences sensitive to BOLD contrast. Each volume consisted of 40 transaxial contiguous sections with a section thickness of 3 mm to cover almost the whole brain (flip angle, 90°; TE, 50 ms; TR, 4 s; matrix, 64 × 64; field of view, 24 cm × 24 cm).

2.4. fMRI data analysis

Data analysis was performed with statistical parametric mapping software 2 (SPM2; Wellcome Department of Cognitive Neurology, University College London, UK) running with MATLAB (Mathworks, Natick, MA). All volumes were realigned to the first volume in each session to correct for head motion and were then spatially normalized to the standard space defined by the Montreal Neurological Institute template. After normalization, all scans had a resolution of 3 mm × 3 mm × 3 mm. Functional images were spatially smoothed with a 3D isotropic Gaussian kernel (full width at half maximum of 8 mm). Low frequency noise was removed by applying a high-pass filter (cutoff period, 80 s) to the fMRI time-series data of each voxel. For subject-level statistical analyses, significant hemodynamic changes in each condition (N, Si, Sc) were examined using the general linear model with boxcar functions convolved with a hemodynamic response function. Statistical parametric maps for each contrast (Si–N, Sc–N, Sc–Si) of the t-statistic were calculated on a voxel-by-voxel basis.

For group comparisons, random effect analyses were performed. The contrast images obtained from subject-level statistical analyses were entered into the random effects analyses. One-sample t-test was performed to determine group activation for each effect. A height threshold of $P < 0.001$ (uncorrected) and an extent threshold of 10 voxels were considered significant. For anatomical localization, peak voxels were converted from MNI to Talairach coordinates (Talairach and Tournoux, 1988).

Please cite this article in press as: Ikeda, Y., et al., Cerebral activation associated with speech sound discrimination during the diotic listening task: An fMRI study. Neurosci. Res. (2010), doi:10.1016/j.neures.2010.02.006

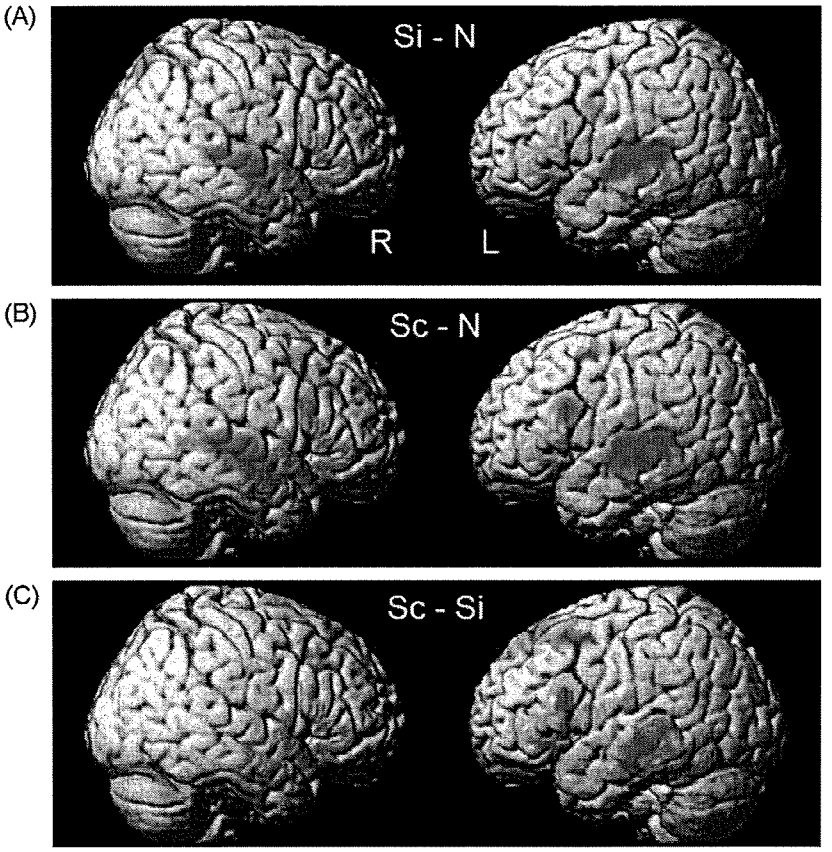

Fig. 2. Cortical rendering of activated areas in selective listening task. (A) Activation in the Si–N constrast. The bilateral temporal, frontal and parietal areas were activated. (B) Activation in the Sc–N contrast. The bilateral temporal, frontal areas, the left insula, cerebellum and the right parietal areas were activated. Compared with Si–N contrast, wider areas were activated in Sc–N contrast. (C) Activation in the Sc–Si contrast. The bilateral temporal, frontal areas and the left parietal areas were activated. All images are shown at the height threshold of $P = 0.001$, uncorrected, and the extent threshold of $k = 10$ voxels.

2.5. Performance analysis of word challenge

Performance score of the word challenge was obtained by counting the number of words that the subjects could answer correctly in the individual conditions with six repetitions. The accuracy rate was expressed as percent of the total number of correct words against all six sequences, and the values were shown as mean ± SD. The accuracy rate was compared among N, Si and Sc conditions using one-way ANOVA, followed by Tukey's multiple comparison test. $P < 0.05$ was considered statistically significant.

Simple regression analyses were performed to examine correlations between task-related BOLD signal changes of Sc–Si contrast and the performance score difference between Si and Sc conditions (Sc–Si). Pearson's correlation coefficient was then calculated with a significance threshold of $P < 0.05$.

3. Results

3.1. fMRI data

To assess the areas activated in selective listening attention under this designed experiment, the BOLD signal changes in both Si–N and Sc–N contrasts were examined. In Si–N contrast, as shown in Fig. 2A, the bilateral STG, middle temporal gyrus (MTG), middle frontal gyrus (MFG), superior parietal lobule (SPL), left precentral gyrus, right inferior frontal gyrus (IFG), precuneus and IPL were significantly activated (Table 1 and Fig. 2A). In Sc–N contrast, there was significant activation in the bilateral STG, MTG, IFG and MFG, the left insula and cerebellum, right medial frontal gyrus, precuneus, supramarginal gyrus (SMG) and inferior parietal gyrus (Table 1 and Fig. 2B). These results suggest that the brain regions activated in Sc condition are more widespread than those in Si condition.

Furthermore, the difference in BOLD signal between Sc and Si conditions was analyzed to reveal how the change of challenge level in speech sound discrimination affects brain hemodynamic activity. In Sc–Si contrast, significant activations were observed in the bilateral STG, MTG, IFG, MFG, medial frontal gyrus, SFG, left inferior temporal gyrus (ITG), SMG and IPL (Table 1 and Fig. 2C).

3.2. Accuracy rate

Next, we investigated whether the difference in challenge level in speech sound discrimination among three conditions reflects the difference in accuracy rate. The subjects judged the presence of the keywords in the preceding narration with 93.3 ± 8.4% (N condition), 92.5 ± 10.1% (Si), and 81.7 ± 17.1% (Sc) of accuracy rates, respectively (ANOVA for group comparison, $P = 0.0065$; Fig. 3). Thus, the subjects answered the target word less correctly in Sc condition than in N and Si conditions ($P < 0.05$), suggesting that they had more difficulty in discriminating the target voice when the distracter was of congruent sex in Sc condition.

3.3. Correlation between fMRI image and performance score

Further, we sought to determine the brain regions responsible for changes of challenge level in speech sound discrimination as measured by BOLD activation. The change in BOLD signal under Sc–Si contrast was positively correlated with the difference in performance score between Si and Sc conditions (Sc–Si) in the left ITG (BA 20, $R = 0.796$, $P < 0.001$), left anterior STG (BA 38, $R = 0.787$,

Please cite this article in press as: Ikeda, Y., et al., Cerebral activation associated with speech sound discrimination during the diotic listening task: An fMRI study. Neurosci. Res. (2010), doi:10.1016/j.neures.2010.02.006

Table 1
Regions activated in selective listening in Si–N, Sc–N and Sc–Si contrasts.

Contrast	Hemisphere	Region (Brodmann area)	Talairach			*t*-Value
			x	*y*	*z*	
Si–N	L	Superior temporal gyrus (22)	−59	−25	7	10.59
		Middle temporal gyrus (21)	−59	−6	−5	6.24
		Precentral gyrus (6/4)	−57	7	31	6.92
		Middle frontal gyrus (46)	−48	42	20	4.13
		Superior parietal lobule (7)	−12	−65	55	4.33
	R	Superior temporal gyrus (22/42)	61	−33	7	5.88
		Middle temporal gyrus (21)	67	−14	−4	5.73
		Middle frontal gyrus (10/9/46)	36	47	11	4.67
		Inferior frontal gyrus (44)	53	13	21	4.34
		Superior parietal lobule (7)	18	−69	50	6.65
		Precuneus (7)	16	−54	52	4.36
		Inferior parietal lobule (40)	57	−42	22	4.04
Sc–N	L	Superior temporal gyrus (22/42)	−51	−17	3	12.08
		Middle temporal gyrus (21)	−53	−12	−6	10.28
		Inferior frontal gyrus (45)	−57	20	19	8.01
		Middle frontal gyrus (6)	−46	4	50	6.24
		Insula	−30	19	−1	4.82
		Cerebellum	−14	−79	−21	5.39
	R	Middle temporal gyrus (21)	61	−6	−11	7.85
		Superior temporal gyrus (22/42)	63	−29	5	6.06
		Inferior frontal gyrus (45/44/47)	59	19	21	6.37
		Middle frontal gyrus (6/10/9/8/46)	48	8	46	5.09
		Medial frontal gyrus (8)	2	37	41	4.18
		Precuneus (7)	14	−62	40	4.85
		Supramarginal gyrus (40)	44	−43	37	4.67
		Inferior parietal lobule (39)	48	−58	43	4.45
Sc–Si	L	Middle temporal gyrus (21)	−55	−20	−7	6.66
		Superior temporal gyrus (22/38)	−46	−23	3	5.7
		Inferior temporal gyrus (20)	−46	−7	−25	4.47
		Inferior frontal gyrus (45/47)	−53	18	14	6.5
		Middle frontal gyrus (8/6)	−32	22	47	6.35
		Medial frontal gyrus (8)	−2	31	46	6.21
		Superior frontal gyrus (8/6)	−8	34	52	5.37
		Supramarginal gyrus (40)	−63	−47	28	5.56
		Inferior parietal lobule (39/40)	−50	−59	23	5.02
	R	Middle temporal gyrus (21)	53	1	−25	4.92
		Superior temporal gyrus (22)	46	−21	3	4.6
		Medial frontal gyrus (8/9)	2	39	40	5.08
		Superior frontal gyrus (8)	8	50	36	4.84
		Inferior frontal gyrus (45)	8	36	52	4.75
		Middle frontal gyrus (8/9/6/46)	61	22	21	4.44

$P<0.001$) and right STG (BA 22, $R=0.722$, $P<0.001$), respectively (Table 2 and Fig. 4). The two subregions in the left temporal gyrus (BA 20 and 38) were also included in activated areas under Sc–Si contrast by the overall analysis as shown in Table 1 (superior temporal gyrus and inferior temporal gyrus). At the individual level, 10 subjects showed no difference in the performance score between Sc and Si conditions, while they had increase in BOLD signal in the left ITG and left anterior STG under Sc–Si contrast (Fig. 4A and B). As for the right STG BOLD signal, seven subjects with lower performance score showed lower BOLD activity in this subregion under Sc condition than Si condition (Fig. 4C).

Table 2
Regions of activation correlated with performance score in Sc–Si contrast.

Hemisphere	Region (Brodmann area)	Talairach			*t*-Value
		x	*y*	*z*	
L	Inferior temporal gyrus (20)	−50	−32	−10	5.31
	Superior temporal gyrus (38)	−48	12	−28	4.46
R	Superior temporal gyrus (22)	63	−8	0	4.66

4. Discussion

4.1. Cortical network in auditory selective attention

By means of fMRI with a diotic experimental paradigm based rather on actual human conversation, cortical hemodynamic response was observed robustly in the bilateral STG and MTG and substantially in the bilateral MFG, right IFG and SPL in both Si and Sc conditions. Brain imaging (PET and fMRI) combined with dichotic listening task (O'Leary et al., 1996; Hugdahl et al., 1999, 2000; Hashimoto et al., 2000; Jäncke et al., 2001, 2003; Hund-Georgiadis et al., 2002) has already been extensively used to reveal the regions responsible for attentive listening. These studies have demonstrated widespread activities not only in the temporal cortex including bilateral STG and MTG, but also in the inferior parietal and prefrontal cortices (Jäncke and Shah, 2002; Lipschutz et al., 2002). In addition, an fMRI study (Nakai et al., 2005) using a diotic listening paradigm has also shown similar brain activation in the frontal association cortex as well as STG. Therefore, brain regions activated during the present diotic listening task are consistent with those previously reported, suggesting that the present task mimicking daily life conditions can efficiently activate the auditory attention networks commonly used during selective listening.

Please cite this article in press as: Ikeda, Y., et al., Cerebral activation associated with speech sound discrimination during the diotic listening task: An fMRI study. Neurosci. Res. (2010), doi:10.1016/j.neures.2010.02.006

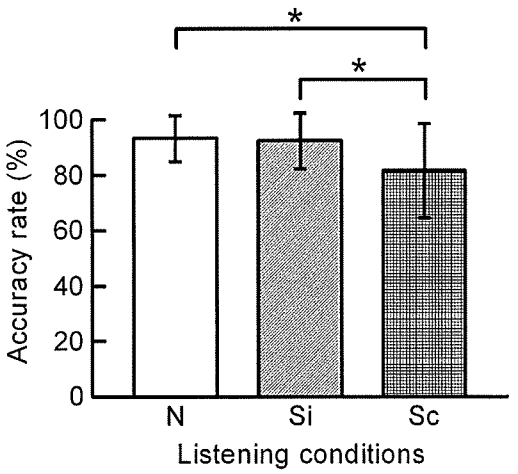

Fig. 3. Accuracy rate of word challenge. The ratio (%) of the number of target words correctly answered by the subjects in the individual conditions in the session was calculated and referred to as accuracy rate. The values were mean ± SD. The accuracy rates were significantly different among the three conditions ($F(2, 57) = 5.5$, $P = 0.0065$). Sc condition has significantly lower accuracy rate compared with N and Si conditions (*$P < 0.05$). N, non-selective listening; Si, selective listening with speakers of incongruent sex; Sc, selective listening with speakers of congruent sex. $n = 20$.

4.2. Diotic selective listening

To accomplish the diotic listening task in the present study, several distinct steps were required to process auditory information: discriminating the voice of the target speaker from that of the distracter, ignoring the distracter's voice, keeping attention focused on the story read by the target speaker, recognizing the words in the story, constructing sentences from the words, and comprehending and memorizing the sentences. In each process, distinct brain regions are thought to be involved. The right anterior part of the superior temporal sulcus and right IFG are reportedly involved in the prosodic component of speech sound processing (Plante et al., 2002; Zatorre et al., 2002) to discriminate the target voice by comparing it with others' prosodic features. The left frontal (BA 6, 8, 9, 44 and 46) and parietal lobes (BA7) have been thought to have a role in ignoring distracter stimuli (Bledowski et al., 2004). Broca's area (BA 44 and 45) is involved in syntactic processing (Stromswold et al., 1996; Caplan et al., 1999). It has been reported that the anterior areas of the left superior temporal gyrus and middle temporal gyrus are involved in speech comprehension (Scott et al., 2000; Davis and Johnsrude, 2003) and the left parietal cortex in working memory retrieval or short-time memory (Majerus et al., 2007; Öztekin et al., 2009). As shown by the results, the present task increased hemodynamic activation in the above-mentioned areas, consistent with the previous observations. Collectively, the present results suggest that the temporal, parietal and frontal regions are extensively involved in overall information processing during selective diotic listening.

However, there are several differences in the activated area between the previous dichotic listening studies and the present results. Activation of the primary auditory area such as BA 41 was not significant at the statistical threshold applied in the present study, while previous dichotic listening task studies found predominant activation in the primary auditory cortex contralateral to the ear of stimulation (Alho et al., 1999; Jäncke et al., 2001). Most of the auditory stimuli adopted in previous dichotic listening task studies were tone and syllables, whereas in the present task we used as stimuli two different contents of sentences read simultaneously but independently by a target and a distracting speaker. Under such condition, the subjects are required to execute neural processes pertaining to lexical access and semantic retrieval for completion of the task. Therefore, the cerebral activation might rather reflect post-sensory linguistic processing. In fact, functional neuroimaging studies using speech as stimuli showed activation of the left-lateralized networks, including the parietal, frontal and temporal cortex (Binder et al., 2009).

In addition, our results showed activation in the bilateral parietal cortices (BA 7) in Si–N contrast, the right parietal cortex (BA 39) in Sc–N contrast, and the left parietal cortex (BA 39 and 40) in Sc–Si contrast. While dichotic listening tasks have been reported to preferentially activate the right parietal cortex in association with spatial auditory processing (Alho and Vorobyev, 2007), left-dominant brain activation has been reported in angular gyrus (BA 39) and its adjacent areas (BA 40 and 7) in the semantic decision task using spoken languages (Binder et al., 1997, 2009). Accordingly, the parietal cortex activation shown in our task may be due to language processing rather than spatial processing.

4.3. Change of challenge level in speech sound discrimination and hemodynamic response in fMRI

As expected from the sex difference in voice properties, Sc condition was more difficult for the subjects to discriminate speech than Si condition when the mean accuracy rate in the performance was compared between Sc and Si conditions. Furthermore, the difference in performance between Si and Sc conditions was positively correlated with the change in BOLD signal under Sc–Si contrast in the left ITG, left anterior and right STG. At the individual level, half of the subjects showed increase in BOLD signal in the left ITG and left anterior STG without apparent difference in performance score between Sc and Si conditions. These results might be interpreted as the subjects making effort to attain good performance, resulting in BOLD increase in these regions. As described above, it has been reported that the left ITG and left anterior STG are involved in lexical–semantic processing (Binder et al., 2009). On the other hand, seven subjects with lower performance score under Sc condition than Si condition showed lower BOLD activity in the right STG. This implies that the activity of this subregion, which reportedly involves sentential prosody processing (Plante et al., 2002; Zatorre et al., 2002), may directly reflect the ability to discriminate performance. The involvement of these regions in successful discrimination may, therefore, indicate that the our present tasks require linguistic processing in addition to phonological one; since targeted words were presented in the news articles, the participants need to comprehend the target speech in the context of the news contents as well as to differentiate the target voice in the context of the phonetic feature. Collectively, these results suggest that these temporal subregions relating to language processing also play important roles in performing speech discrimination under constantly changing auditory conditions intermingled with different speakers' voices.

4.4. Selective auditory attention and psychiatric disorders

Patients with psychiatric disorders are known to often suffer from attention disturbance. For instance, deficit in attention has been thought to be a primary feature of neurocognitive profiles of patients with schizophrenia on the basis of neuropsychological studies (Heinrichs and Zakzanis, 1998; Fioravanti et al., 2005). Intriguingly, functional imaging studies of attention and working memory, however, have reported mixed findings in these patients. Attention task-related activation is attenuated in schizophrenia in DLPFC (Ojeda et al., 2002) and STG (Gallinat et al., 2002) as compared to in healthy subjects. In contrast, enhanced activa-

Please cite this article in press as: Ikeda, Y., et al., Cerebral activation associated with speech sound discrimination during the diotic listening task: An fMRI study. Neurosci. Res. (2010), doi:10.1016/j.neures.2010.02.006

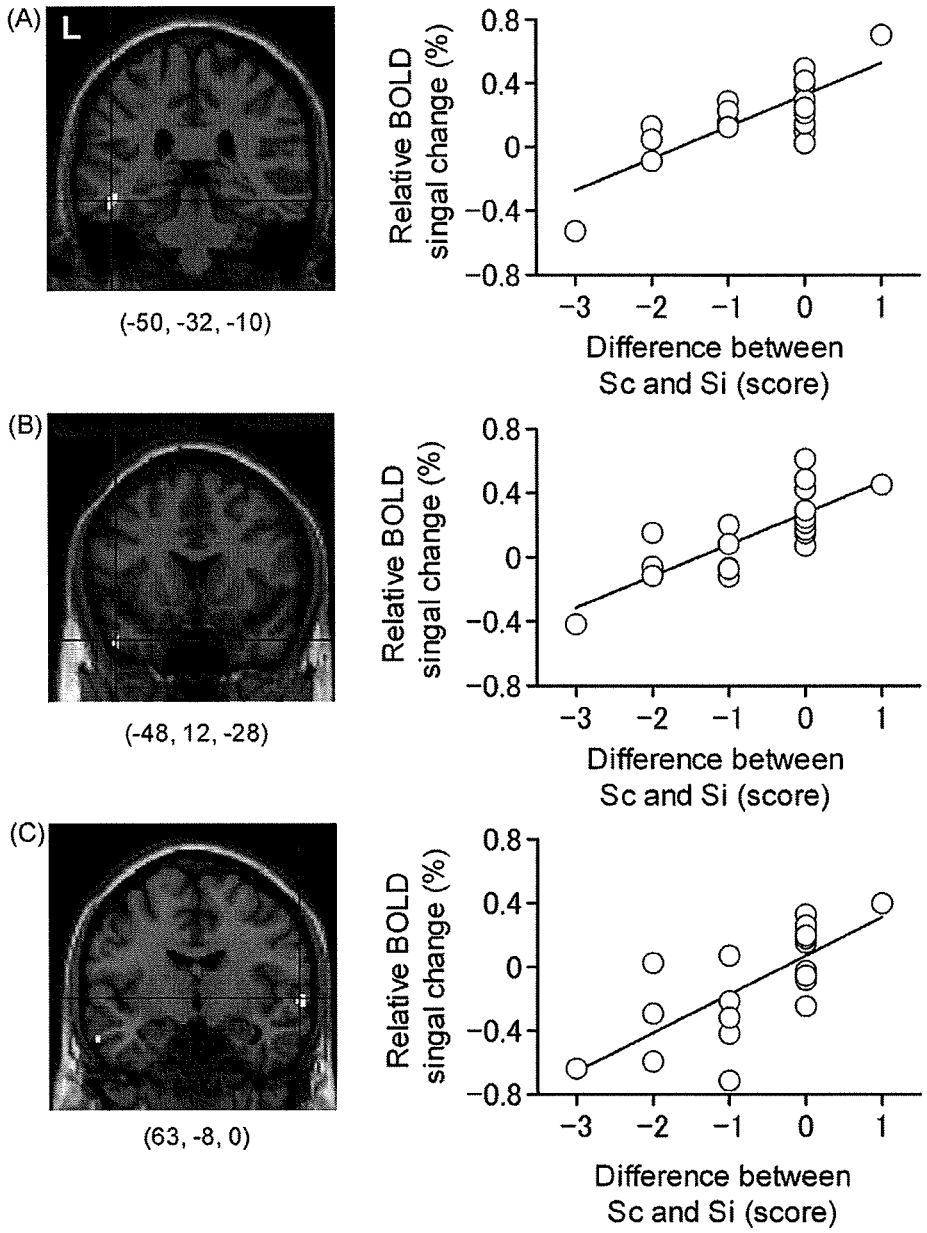

Fig. 4. Correlation between relative BOLD signal change and performance score difference in Sc–Si contrast. In the right panels, the vertical axes represent relative BOLD signal change in Sc–Si contrast, and the horizontal axes indicate the difference in performance score between Si and Sc conditions. Scatter plots illustrate significant positive correlations by simple regression analyses between neural activation of the left inferior temporal gyrus (A), left anterior superior temporal gyrus (B), or right superior temporal gyrus (C) and the performance score difference (Sc–Si). The left panels illustrate the brain regions with corresponding Talairach coordinates showing the correlations as described.

tion in DLPFC (Weiss et al., 2003) and STG (Weiss et al., 2007; Schirmer et al., 2009) has been observed in schizophrenia. Such discrepancy may be derived not only from the wide variety of patient profiles, but also task designs, which focus on different aspects of neurocognitive function of patients. A key feature of the paradigm used in the present study is that it could uniquely depict the brain activity during listening attention encountered in the daily conversational environment. In addition, this task can measure an activity change of the speech sound discrimination in temporal areas, which is reportedly reduced in volume in patients with schizophrenia (Collinson et al., 2009; Sun et al., 2009). Therefore, future studies using the present diotic task may be useful for investigating the cognitive aspect of auditory attention in patients with attention disturbance such as schizophrenia.

Acknowledgments

We thank the staffs of Asai hospital for their assistance in collecting the demographic data. Funding for this study was provided by a Grant-in-Aid for Science Research (C) from the Ministry of Education, Culture, Sports, Science, and Technology (MEXT), Japan, to H.S. (no. 1659028), a Grant-in-Aid for Encouragement of Young Scientists (B) from the Japan Society for the Promotion of Science (JSPS) to N.Y. (no. 18790852) and to Y.I. (no. 17790821).

References

Alho, K., Medvedev, S.V., Pakhomov, S.V., Roudas, M.S., Tervaniemi, M., Reinikainen, K., Zeffiro, T., Näätänen, R., 1999. Selective tuning of the left and right auditory cortices during spatially directed attention. Cogn. Brain Res. 7, 335–341.

Please cite this article in press as: Ikeda, Y., et al., Cerebral activation associated with speech sound discrimination during the diotic listening task: An fMRI study. Neurosci. Res. (2010), doi:10.1016/j.neures.2010.02.006

Alho, K., Vorobyev, V.A., 2007. Brain activity during selective listening to natural speech. Front. Biosci. 12, 3167–3176.
Beaman, C.P., Bridges, A.M., Scott, S.K., 2007. From dichotic listening to the irrelevant sound effect: a behavioural and neuroimaging analysis of the processing of unattended speech. Cortex 43, 124–134.
Binder, J.R., Frost, J.A., Hammeke, T.A., Cox, R.W., Rao, S.M., Prieto, T., 1997. Human brain language areas identified by functional magnetic resonance imaging. J. Neurosci. 17, 353–362.
Binder, J.R., Desai, R.H., Graves, W.W., Conant, L.L., 2009. Where is the semantic system? A critical review and meta-analysis of 120 functional neuroimaging studies. Cereb. Cortex 19, 2767–2796.
Bledowski, C., Prvulovic, D., Goebel, R., Zanella, F.E., Linden, D.E.J., 2004. Attentional systems in target and distractor processing: a combined ERP and fMRI study. Neuroimage 22, 530–540.
Bryden, M.P., 1988. Correlates of the dichotic right-ear effect. Cortex 24, 313–319.
Caplan, D., Alpert, N., Waters, G., 1999. PET studies of syntactic processing with auditory sentence presentation. Neuroimage 9, 343–351.
Chen, S.H., 2007. Sex differences in frequency and intensity in reading and voice range profiles for Taiwanese adult speakers. Folia Phoniatr. Logop. 59, 1–9.
Collinson, S.L., Mackay, C.E., Jiaqing, O., James, A.C.D., Crow, T.J., 2009. Dichotic listening impairments in early onset schizophrenia are associated with reduced left temporal lobe volume. Schizophr. Res. 112, 24–31.
Davis, M.H., Johnsrude, I.S., 2003. Hierarchical processing in spoken language comprehension. J. Neurosci. 23, 3423–3431.
Fioravanti, M., Carlone, O., Vitale, B., Cinti, M.E., Clare, L., 2005. A meta-analysis of cognitive deficits in adults with a diagnosis of schizophrenia. Neuropsychol. Rev. 15, 73–95.
Gallinat, J., Mulert, C., Bajbouj, M., Herrmann, W.M., Schunter, J., Senkowski, D., Moukhtieva, R., Kronfeldt, D., Winterer, G., 2002. Frontal and temporal dysfunction of auditory stimulus processing in schizophrenia. Neuroimage 17, 110–127.
Grady, C.L., Van Meter, J.W., Maisog, J.M., Pietrini, P., Krasuski, J., Rauschecker, J.P., 1997. Attention-related modulation of activity in primary and secondary auditory cortex. Neuroreport 8, 2511–2516.
Hashimoto, R., Homae, F., Nakajima, K., Miyashita, Y., Sakai, K.L., 2000. Functional differentiation in the human auditory and language areas revealed by a dichotic listening task. Neuroimage 12, 147–158.
Heinrichs, R.W., Zakzanis, K.K., 1998. Neurocognitive deficit in schizophrenia: a quantitative review of the evidence. Neuropsychology 12, 426–445.
Hugdahl, K., Brønnick, K., Kyllingsbæk, S., Law, I., Gade, A., Paulson, O.B., 1999. Brain activation during dichotic presentations of consonant–vowel and musical instrument stimuli: a ^{15}O-PET study. Neuropsychologia 37, 431–440.
Hugdahl, K., Law, I., Kyllingsbæk, S., Brønnick, K., Gade, A., Paulson, O.B., 2000. Effects of attention on dichotic listening: an ^{15}O-PET study. Hum. Brain Mapp. 10, 87–97.
Hund-Georgiadis, M., Lex, U., Friederici, A.D., von Cramon, D.Y., 2002. Non-invasive regime for language lateralization in right- and left-handers by means of functional MRI and dichotic listening. Exp. Brain Res. 145, 166–176.
Jäncke, L., Buchanan, T.W., Lutz, K., Shah, N.J., 2001. Focused and nonfocused attention in verbal and emotional dichotic listening: an FMRI study. Brain Lang. 78, 349–363.
Jäncke, L., Shah, N.J., 2002. Does dichotic listening probe temporal lobe functions? Neurology 58, 736–743.
Jäncke, L., Specht, K., Shah, J.N., Hugdahl, K., 2003. Focused attention in a simple dichotic listening task: an fMRI experiment. Cogn. Brain Res. 16, 257–266.
Kimura, D., 1961. Cerebral dominance and the perception of verbal stimuli. Can. J. Psychol. 15, 166–171.
Lipschutz, B., Kolinsky, R., Damhaut, P., Wikler, D., Goldman, S., 2002. Attention-dependent changes of activation and connectivity in dichotic listening. Neuroimage 17, 643–656.
Majerus, S., Bastin, C., Poncelet, M., Van der Linden, M., Salmon, E., Collette, F., Maquet, P., 2007. Short-term memory and the left intraparietal sulcus: focus of attention? Further evidence from a face short-term memory paradigm. Neuroimage 35, 353–367.
Nakai, T., Kato, C., Matsuo, K., 2005. An fMRI study to investigate auditory attention: a model of the cocktail party phenomenon. Magn. Reson. Med. Sci. 4, 75–82.
Ojeda, N., Ortuño, F., Arbizu, J., López, P., Martí-Climent, J.M., Peñuelas, I., Cervera-Enguix, S., 2002. Functional neuroanatomy of sustained attention in schizophrenia: contribution of parietal cortices. Hum. Brain Mapp. 17, 116–130.
O'Leary, D.S., Andreasen, N.C., Hurtig, R.R., Hichwa, R.D., Watkins, G.L., Ponto, L.L.B., Rogers, M., Kirchner, P.T., 1996. A positron emission tomography study of binaurally and dichotically presented stimuli: effects of level of language and directed attention. Brain Lang. 53, 20–39.
Oldfield, R.C., 1971. The assessment and analysis of handedness: the Edinburgh inventory. Neuropsychologia 9, 97–113.
Öztekin, I., McElree, B., Staresina, B.P., Davachi, L., 2009. Working memory retrieval: contributions of the left prefrontal cortex, the left posterior parietal cortex, and the hippocampus. J. Cogn. Neurosci. 21, 581–593.
Petkov, C.I., Kang, X., Alho, K., Bertrand, O., Yund, E.W., Woods, D.L., 2004. Attentional modulation of human auditory cortex. Nat. Neurosci. 7, 658–663.
Plante, E., Creusere, M., Sabin, C., 2002. Dissociating sentential prosody from sentence processing: activation interacts with task demands. Neuroimage 17, 401–410.
Pugh, K.R., Shaywitz, B.A., Shaywitz, S.E., Fulbright, R.K., Byrd, D., Skudlarski, P., Shankweiler, D.P., Katz, L., Constable, R.T., Fletcher, J., Lacadie, C., Marchione, K., Gore, J.C., 1996. Auditory selective attention: an fMRI investigation. Neuroimage 4, 159–173.
Schirmer, T.N., Dorflinger, J.M., Marlow-O'Connor, M., Pendergrass, J.C., Hartzell, A., All, S.D., Charles, D., 2009. FMRI indices of auditory attention in schizophrenia. Prog. Neuropsychopharmacol. Biol. Psychiatry 33, 25–32.
Scott, S.K., Blank, C.C., Rosen, S., Wise, R.J.S., 2000. Identification of a pathway for intelligible speech in the left temporal lobe. Brain 123, 2400–2406.
Scott, S.K., Rosen, S., Wichham, L., Wise, R.J.S., 2004. A positron emission tomography study of the neural basis of informational and energetic masking effects in speech perception. J. Acoust. Soc. Am. 115, 813–821.
Shafiro, V., Gygi, B., 2007. Perceiving the speech of multiple concurrent talkers in a combined divided and selective attention task. J. Acoust. Soc. Am. 122, EL229–EL235.
Stromswold, K., Caplan, D., Alpert, N., Rauch, S., 1996. Localization of syntactic comprehension by positron emission tomography. Brain Lang. 52, 452–473.
Sun, J., Maller, J.J., Guo, L., Fitzgerald, P.B., 2009. Superior temporal gyrus volume change in schizophrenia: a review on region of interest volumetric studies. Brain Res. Rev. 61, 14–32.
Talairach, J., Tournoux, P., 1988. Co-planar Stereotaxic Atlas of the Human Brain: 3-Dimensional Proportional System—An Approach to Cerebral Imaging. Thieme Medical Publishers, New York.
Thomsen, T., Rimol, L.M., Ersland, L., Hugdahl, K., 2004. Dichotic listening reveals functional specificity in prefrontal cortex: an fMRI study. Neuroimage 21, 211–218.
Tzourio, N., Massioui, F.E., Crivello, F., Joliot, M., Renault, B., Mazoyer, B., 1997. Functional anatomy of human auditory attention studied with PET. Neuroimage 5, 63–77.
van den Noort, M., Specht, K., Rimol, L.M., Ersland, L., Hugdahl, K., 2008. A new verbal reports fMRI dichotic listening paradigm for studies of hemispheric asymmetry. Neuroimage 40, 902–911.
Weiss, E.M., Golaszewski, S., Mottaghy, F.M., Hofer, A., Hausmann, A., Kemmler, G., Kremser, C., Brinkhoff, C., Felber, S.R., Fleischhacker, W.W., 2003. Brain activation patterns during a selective attention test—a functional MRI study in healthy volunteers and patients with schizophrenia. Psychiatry Res. Neuroimaging 123, 1–15.
Weiss, E.M., Siedentopf, C., Golaszewski, S., Mottaghy, F.M., Hofer, A., Kremser, C., Felber, S., Fleischhacker, W.W., 2007. Brain activation patterns during a selective attention test—a functional MRI study in healthy volunteers and unmedicated patients during an acute episode of schizophrenia. Psychiatry Res. Neuroimaging 154, 31–40.
Zatorre, R.J., Mondor, T.A., Evans, A.C., 1999. Auditory attention to space and frequency activates similar cerebral systems. Neuroimage 10, 544–554.
Zatorre, R.J., Belin, P., Penhune, V.B., 2002. Structure and function of auditory cortex: music and speech. Trends Cogn. Sci. 6, 37–46.

Please cite this article in press as: Ikeda, Y., et al., Cerebral activation associated with speech sound discrimination during the diotic listening task: An fMRI study. Neurosci. Res. (2010), doi:10.1016/j.neures.2010.02.006

Journal of Nuclear Medicine, published on April 16, 2009 as doi:10.2967/jnumed.108.058503

Quantitative PET Analysis of the Dopamine D_2 Receptor Agonist Radioligand ^{11}C-(*R*)-2-CH_3O-*N*-n-Propylnorapomorphine in the Human Brain

Tatsui Otsuka[1,2], Hiroshi Ito[1], Christer Halldin[3], Hidehiko Takahashi[1], Harumasa Takano[1], Ryosuke Arakawa[1], Masaki Okumura[1], Fumitoshi Kodaka[1], Michie Miyoshi[1], Mizuho Sekine[1], Chie Seki[1], Ryuji Nakao[4], Kazutoshi Suzuki[4], Sjoerd Finnema[3], Yoshio Hirayasu[2], Tetsuya Suhara[1], and Lars Farde[3]

[1]*Molecular Neuroimaging Group, Molecular Imaging Center, National Institute of Radiological Sciences, Chiba, Japan;* [2]*Department of Psychiatry, Yokohama City University School of Medicine, Yokohama, Japan;* [3]*Psychiatry Section, Department of Clinical Neuroscience, Karolinska Institutet, Karolinska Hospital, Stockholm, Sweden; and* [4]*Molecular Probe Group, Molecular Imaging Center, National Institute of Radiological Sciences, Chiba, Japan*

It has been demonstrated in vitro that the dopamine D_2 receptor has 2 interconvertible affinity states for endogenous dopamine, referred to as the high- and the low-affinity states. ^{11}C-(*R*)-2-CH_3O-*N*-n-propylnorapomorphine (^{11}C-MNPA) is a new agonist radioligand for in vivo imaging of the high-affinity state of dopamine D_2 receptors using PET. In the present study, the kinetics of ^{11}C-MNPA were examined for the first time, to our knowledge, in the human brain and analyzed using quantitative approaches with or without an arterial input function. **Methods:** A 90-min dynamic PET scan was obtained for 10 healthy men after an intravenous injection of ^{11}C-MNPA. The binding potential (BP_{ND}) was calculated using the indirect kinetic method, a kinetic compartment analysis with a metabolite-corrected arterial input function. BP_{ND} was also calculated by the simplified reference tissue model (SRTM) and transient equilibrium methods, both with the cerebellum as the reference brain region. The results of the quantitative methods were compared in a cross-validation approach. **Results:** The highest regional radioactivity was observed in the putamen. BP_{ND} values obtained by kinetic analysis were 0.82 ± 0.09, 0.59 ± 0.11, and 0.28 ± 0.06, respectively, in the putamen, caudate, and thalamus. BP_{ND} values obtained by the SRTM and transient equilibrium methods were in good agreement with those obtained by the indirect kinetic method (r = 0.98 and r = 0.93, respectively). For all quantification methods, the BP_{ND} values based on data acquired from 0 to 60 min were in good agreement with those based on data acquired from 0 to 90 min (r = 0.90–0.99). **Conclusion:** The regional distribution of ^{11}C-MNPA binding was in good agreement with previous PET studies of dopamine D_2 receptors in the human brain using antagonist radioligands. The results support routine use of the SRTM and transient equilibrium methods, that is, methods that do not require an arterial input function and need a scan time of only about 60 min. ^{11}C-MNPA should thus be useful for clinical research on the pathophysiology of neuropsychiatric disorders and estimation of dopamine D_2 receptor occupancy by dopaminergic drugs.

Key Words: ^{11}C-MNPA; agonist; dopamine D_2 receptor; positron emission tomography; human

J Nucl Med 2009; 50:703–710
DOI: 10.2967/jnumed.108.058503

The dopaminergic system in the brain plays a significant role in the physiologic regulation of motor functions, cognition, emotion, and personality (*1*). Alterations of dopaminergic neurotransmission have been implicated in several pathologic conditions, such as schizophrenia (*2*), Parkinson disease (*3*), and addiction (*4*). Dopamine receptors are classified into 5 subtypes, D_1, D_2, D_3, D_4, and D_5 (*5*). The dopamine D_2 receptor is a main therapeutic target for currently used antipsychotic drugs and has long been suggested to be involved in the pathophysiology of schizophrenia (*2,6–11*).

Several observations in vitro indicate that the dopamine D_2 receptor exists in 2 interconvertible affinity states, distinguished by the affinity of endogenous dopamine and referred to as the high- and low-affinity states. It has further been suggested that the high-affinity state is the functionally active form of the receptor and is thus more relevant for clinical studies (*12*). Studies of dopamine D_2 receptors using PET have almost exclusively been performed with antagonist radioligands, such as ^{11}C-raclopride and ^{11}C-FLB457 (*13–15*). Antagonist radioligands do, however, bind with equal affinity to the 2 conformational states of the dopamine D_2 receptor. To examine the high-affinity state of the dopamine D_2 receptor in vitro and in vivo, agonist radioligands such as (−)-*N*-^{11}C-propyl-norapomorphine

Received Sep. 25, 2008; revision accepted Jan. 21, 2009.
For correspondence or reprints contact: Hiroshi Ito, Molecular Neuroimaging Group, Molecular Imaging Center, National Institute of Radiological Sciences 4-9-1, Anagawa, Inage-ku, Chiba, 263-8555, Japan.
E-mail: hito@nirs.go.jp

(^{11}C-NPA) and ^{11}C-(+)-4-propyl-3,4,4a,5,6,10b-hexahydro-2H-naphtho[1,2-b][1,4]oxazin-9-ol (^{11}C-PHNO) have recently been developed (*16,17*).

^{11}C-(*R*)-2-CH_3O-*N*-n-propylnorapomorphine (^{11}C-MNPA) is another new agonist PET radioligand with high affinity and selectivity for the dopamine D_2 receptor (inhibitory concentration of 50%, 1.02 nM; inhibition constant 0.17 nM, respectively) (*18,19*) and was recently characterized in nonhuman primates (*20*). PET measurements in cynomolgus monkeys showed high uptake in the striatum, with a striatum-to-cerebellum ratio of 2:2. The striatal uptake of ^{11}C-MNPA could be inhibited by the injection of unlabeled raclopride, confirming that the striatal binding is reversible and specific for dopamine D_2 receptors. Subsequent applied studies using amphetamine-induced dopamine release showed that ^{11}C-MNPA was more sensitive than ^{11}C-raclopride, thus supporting the indication that ^{11}C-MNPA is a promising radioligand for PET of the high-affinity state of the dopamine D_2 receptor in vivo (*21*). The aim of the present study was to examine the regional distribution and kinetics of ^{11}C-MNPA in the human brain. Ten control subjects were included, and data were analyzed using kinetic compartment analyses with a metabolite-corrected input function and 2 quantitative methods with the cerebellum as a reference brain region.

MATERIALS AND METHODS

Subjects

Ten healthy men (age range, 22–35 y; mean ± SD, 27.7 ± 5.4y) participated in this study. On the basis of their medical history and MRI of the brain, all subjects were free of any somatic, neurologic, or psychiatric disorders, and they had no history of current or previous drug abuse. Written informed consent was obtained from all subjects after the study was completely described. The study was approved by the Ethics and Radiation Safety Committee of the National Institute of Radiological Sciences, Chiba, Japan.

PET Procedure

^{11}C-MNPA was synthesized as described in detail previously (*20*). In brief, ^{11}C-MNPA was synthesized by the methylation of (*R*)-(−)-2,10,11-trihydroxy-*N*-n-propylnoraporphine-acetonide with ^{11}C-methyl triflate and subsequent cleavage of the acetonide protecting group with the addition of hydrochloric acid. An ECAT EXACT HR+ PET system (CTI-Siemens) was used for all measurements. A head-fixation device was used to minimize head movements during data acquisition. A transmission scan for attenuation correction was obtained using a ^{68}Ge–^{68}Ga source. Dynamic PET scans were obtained after a 1-min intravenous slow bolus injection of ^{11}C-MNPA (204.3–232.1 MBq; mean ± SD, 219.3 ± 8.2 MBq). The specific radioactivity of ^{11}C-MNPA was 197.5–335.0 GBq/μmol (261.1 ± 43.3 GBq/μmol) at the time of injection. Brain radioactivity was measured from 0 to 90 min (20 s × 9, 1 min × 5, 2 min × 4, 4 min × 11, and 5 min × 6).

MR images of the brain were acquired with a 1.5-T MRI scanner (Gyroscan NT; Philips). T1-weighted images were obtained at 1-mm slices acquired in 3 dimensions.

Arterial Blood Sampling and Metabolite Analysis

To obtain the arterial input function, a series of arterial blood samples were taken manually from a catheter 32 times (2.5 mL × 22 times for the measurement of radioactivity concentration in whole blood and plasma; 5.0 mL × 10 times for the determination of the percentage of unchanged ^{11}C-MNPA in plasma) during the 90-min PET scan. Each blood sample was centrifuged to obtain plasma and blood cell fractions, and the concentrations of radioactivity in whole blood and plasma were measured.

The percentage of unchanged ^{11}C-MNPA in plasma was determined by high-performance liquid chromatography (HPLC) in 10 of the blood samples. Acetonitrile was added to each plasma sample, and the samples were then centrifuged. The supernatant was subjected to radio-HPLC analysis (column, XBridge Prep C18; Waters) (mobile phase, 48:52 90% acetonitrile:50 mM ammonium acetate). The arterial plasma input function was defined as the radioactivity of plasma multiplied by the percentage of unchanged radioligand.

Regions of Interest (ROIs)

All MR images were coregistered to the PET images using the statistical parametric mapping system (SPM2; Wellcome Trust Centre for Neuroimaging) (*22*). ROIs were drawn manually on summated PET images with reference to the coregistered MR images. ROIs were defined for the cerebellar cortex, putamen, caudate, and thalamus. Regional radioactivity was calculated for each frame, corrected for decay, and plotted versus time.

Kinetic Compartment Analysis of ^{11}C-MNPA Binding

To describe the kinetics of ^{11}C-MNPA in the brain, the 2-tissue-compartment model with 4 rate constants, K_1, k_2, k_3, and k_4, was used. The 3 compartments include C_P, the radioactivity concentration of unchanged radioligand in plasma (arterial input function); C_{ND}, the radioactivity concentration of nondisplaceable radioligand in the brain (including nonspecifically bound and free radioligand); and C_S, the radioactivity concentration of radioligand specifically bound to receptors. The rate constants K_1 and k_2 represent the influx and efflux rates for radioligand diffusion across the blood–brain barrier. The rate constants k_3 and k_4 represent radioligand transfer between the compartments for nondisplaceable and specifically bound radioligand.

Calculation of the ^{11}C-MNPA Binding Potential

^{11}C-MNPA binding was expressed by the indirect kinetic, SRTM, and transient equilibrium methods. In these methods, ^{11}C-MNPA bindings were expressed as binding relative to nondisplaceable binding (BP_{ND}) (*23*). The BP_{ND} of the radioligand is proportional to the product of the receptor density (B_{max}) and reciprocal affinity ($1/K_d$), and the ratio of B_{max} to K_d corresponds to the ratio of k_3 to k_4, as expressed by the following equation:

$$BP_{ND} = f_{ND}(B_{max}/K_d) = k_3/k_4, \qquad \text{Eq. 1}$$

where f_{ND} is the free fraction of radioligand in the nondisplaceable compartment. The cerebellum (cerebellar cortex) was used as a reference brain region because it is a structure with negligible D_2 dopamine receptor density (*24*). The software package PMOD (PMOD Technologies) was used for the indirect kinetic, SRTM, and transient equilibrium quantitative methods.

Indirect Kinetic Method. In the present cross-validation approach, the indirect kinetic method was used as the standard method (*25*). BP_{ND} was defined as the ratio of k_3 to k_4 as calculated using the 2-tissue-compartment model. Because the ratio of k_3 to k_4 is sensitive for noise in the PET data, BP_{ND} was

calculated using the indirect kinetic method. With the cerebellum as a reference region, BP_{ND} can be expressed as:

$$BP_{ND} = V_{T(region)}/V_{T(cerebellum)} - 1, \quad \text{Eq. 2}$$

where $V_{T(region)}$ is the total distribution volume ($= (K_1/k_2)(k_3/k_4 + 1)$) in a target region, and $V_{T(cerebellum)}$ is the total distribution volume ($= K_1/k_2$) in the cerebellum. The rate constants K_1, k_2, k_3, and k_4 in the putamen, caudate, and thalamus were determined by nonlinear curve fitting in a least-squares sense to the regional time–activity curves as described in the literature (*15*). K_1 and k_2 values in the cerebellum were also determined by nonlinear curve fitting in a least-squares sense but by using the 1-tissue-compartment model, assuming that the cerebellum has negligible D_2 dopamine receptor density (*24*). To improve the stability of the curve fitting in the nonlinear curve-fitting procedure, the ratio of K_1 to k_2 was fixed for each subject to the value obtained in the cerebellum by the kinetic analysis with the 1-tissue-compartment model (range of K_1/k_2, 5.0–7.9 mL/cm^3; mean ± SD, 6.5 ± 0.75 mL/cm^3). In this analysis, blood volume, which depends on the first-pass extraction fraction of the tracer, was estimated using the radioactivity of whole blood to diminish the influence of tracer remaining in the blood (*26*).

SRTM Method. The SRTM method, assuming that both target and reference regions have the same level of nondisplaceable binding, can be used to interpret time–activity curves in the target region as follows (*27*):

$$C_T(t) = R_1C_R(t) + (k_2 - R_1k_2/(1+BP_{ND}))C_R(t) * \exp(-k_2t/(1+BP_{ND})), \quad \text{Eq. 3}$$

where $C_T(t)$ is the total radioactivity concentration in a brain region measured by PET, R_1 is the ratio of K_1 to K_1' (K_1, influx rate constant for the brain region; K_1', influx rate constant for the reference region), $C_R(t)$ is the radioactivity concentration in the reference region (cerebellum), and * denotes the convolution integral. The parameters R_1, k_2, and BP_{ND} in this model were estimated by the nonlinear curve-fitting procedure.

Transient Equilibrium Method. Transient equilibrium theoretically occurs when the derivative for specific binding ($dC_S(t)/dt$) is 0, that is, the peak point of specific binding, $C_S(t)$ (*15,28*). It follows that $C_S(t)/C_{ND}(t)$ is equal to k_3/k_4 ($= BP_{ND}$) at transient equilibrium.

Simulation Study

A simulation study was performed to estimate errors of BP_{ND} calculated by the SRTM and transient equilibrium methods. The assumed values and intervals examined were acquired from the results of the kinetic approach. Regional tissue time–activity curves (0–90 min) were generated according to the 2-tissue-compartment model. We assumed that the value of K_1/k_2 equaled 6.6 mL/cm^3 and that of k_4 equaled 0.18 min^{-1}. The tissue time–activity curves were generated with K_1 values between 0.20 and 0.60 mL/cm^3/min in 6 steps and with k_3 values between 0.02 and 0.20 min^{-1} in 10 steps. A tissue time–activity curve for the cerebellum was generated according to the 1-tissue-compartment model with 2 rate constants, using 0.44 mL/cm^3/min for K_1 and 0.067 min^{-1} for k_2. The average arterial input function ($n = 10$), corrected for labeled metabolites, was used to generate the tissue time–activity curves. BP_{ND} was then calculated by applying the SRTM and transient equilibrium methods to the generated tissue time–activity curves. The estimated BP_{ND} values were compared with the BP_{ND} values calculated by the indirect kinetic method.

Variations in K_1 values between a brain region and the cerebellum due to differences in cerebral blood flow (CBF) between

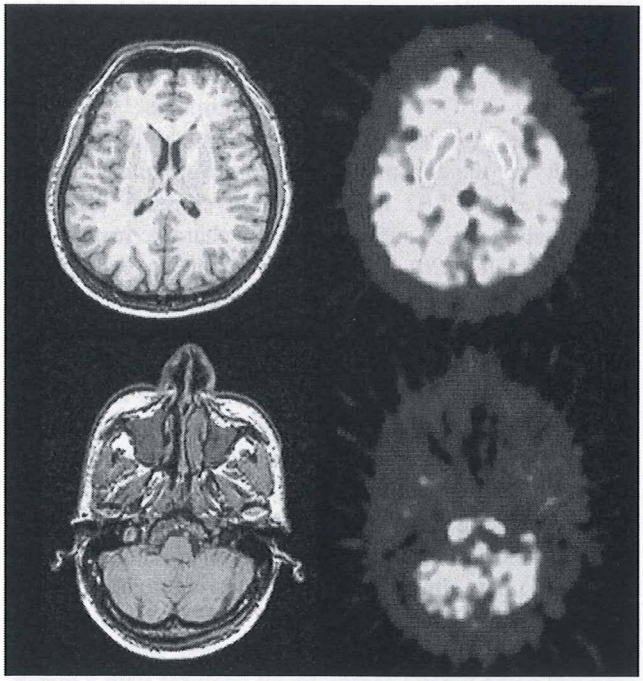

RGB

FIGURE 1. Representative summated PET images 60–90 min after intravenous injection of ^{11}C-MNPA (221 MBq) and corresponding T1-weighted MR images in control human subject. Upper panel shows horizontal section through striatum, and lower panel shows section through cerebellum.

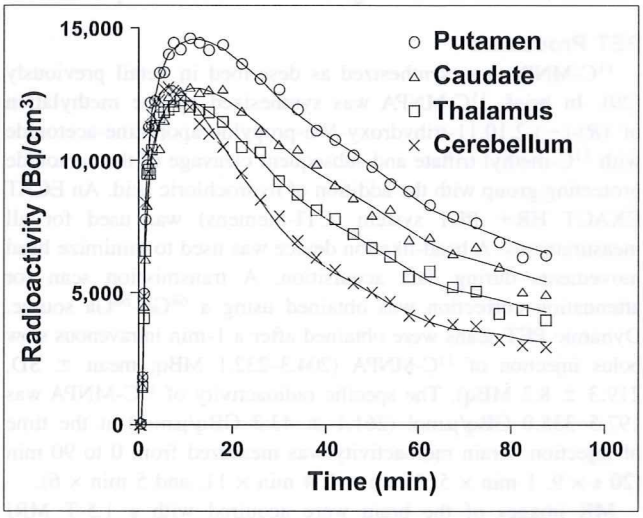

FIGURE 2. Representative regional time–activity curves after intravenous injection of ^{11}C-MNPA (232 MBq) binding in control human subject. Fitted curves using 2-tissue- and 1-tissue-compartment models are also shown for target regions and cerebellum, respectively.

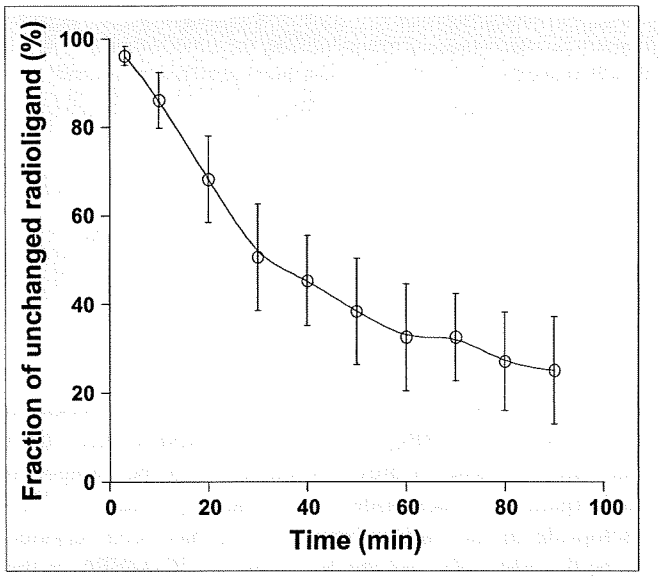

FIGURE 3. Average (n = 10) percentage of unchanged ^{11}C-MNPA in plasma vs. time. Bars indicate SD.

the 2 regions might affect the BP_{ND} calculated by the SRTM and transient equilibrium methods. Furthermore, changes in K_1 due to changes in CBF might be caused by neurologic or psychiatric diseases. The K_1 value for ^{11}C-MNPA was about 0.44 mL/cm^3/min in gray matter. When the CBF value in gray matter is assumed to be 0.50 mL/cm^3/min (*29*), the first-pass extraction fraction of ^{11}C-MNPA is 88%. The capillary permeability–surface area product (PS) value, using this extraction fraction and a K_1 value of 0.44 mL/cm^3/min, was calculated (*30,31*). With the PS value of 1.06 mL/cm^3/min, the K_1 range of 0.20–0.60 mL/cm^3/min corresponds to the CBF range of 0.20–0.85 mL/cm^3/min (*28*).

RESULTS

All 10 subjects participated in the study according to the protocol. Representative summated PET images (60–90 min) and T1-weighted MR images are shown in Figure 1, and the corresponding regional time–activity curves are shown in Figure 2. Regional radioactivity was highest in the putamen and lower in the caudate and thalamus. The average percentage of unchanged ^{11}C-MNPA in plasma was 95.1% ± 2.1% at 3 min, decreasing to 25.1% ± 12.0% at 90 min (i.e., at the end of PET data acquisition) (Fig. 3). Other than MNPA, there were no more lipophilic-labeled metabolites in the plasma.

After an intravenous injection of ^{11}C-MNPA, total radioactivity in the brain peaked at 6.7 ± 1.2 min (range, 4.5–9.0 min), and the fraction of uptake in the brain was 6.0% ± 1.0% (range, 4.3%–7.3%) of the injected radioactivity.

The blood volume and rate constants for each brain region obtained by conventional nonlinear least-squares fit of the 2-compartment model are shown in Table 1. The BP_{ND} values of the putamen, caudate, and thalamus calculated by the 3 different methods are shown in Table 2. Specific binding, as defined by the transient equilibrium method, reached a peak within 60 min in the putamen, caudate, and thalamus (Table 2).

BP_{ND} values determined by the SRTM method on the basis of data acquired for 90 and 60 min and those determined by the transient equilibrium method were compared with values calculated by the indirect kinetic method. BP_{ND} values obtained by the SRTM method were in good agreement with those obtained by the indirect kinetic method with data obtained for 90 and 60 min (Fig. 4), and BP_{ND} values obtained by the transient equilibrium method were in good agreement with those obtained by the indirect kinetic method with data for 90 min (Fig. 5). The highest coefficient of correlation was observed between the SRTM and the indirect kinetic methods with data acquired for 90 min (r = 0.98, $P < 0.001$).

When BP_{ND} values determined by the indirect kinetic and SRTM methods with 60-min data were compared with values determined by the same 2 methods with 90-min data, good agreement was observed (r = 0.99, r = 0.92, $P < 0.001$) (Fig. 6).

To estimate the sensitivity of the SRTM and transient equilibrium methods for rate constants (indirect blood flow) over an interval with values lower and higher than average, a simulation study was performed. BP_{ND} values determined by the indirect kinetic method with data acquired for 60 and 90 min were compared with BP_{ND} values determined by the SRTM and transient equilibrium methods with data acquired for 60 and 90 min from simulated time–activity curves. The error in BP_{ND} calculated by the SRTM method with data acquired for 90 min was smallest (−24.8% to 1.5%; mean, −4.3%), and the difference in K_1 between the brain region and cerebellum had only a minor effect on

TABLE 1. Rate Constants Obtained by Conventional Nonlinear Least-Squares Fit of 2-Tissue-Compartment Model

Region	Blood volume	Rate constant			
		K_1 (mL/cm^3/min)	k_2 (min^{-1})	k_3 (min^{-1})	k_4 (min^{-1})
Putamen	0.07 ± 0.02	0.44 ± 0.05	0.07 ± 0.01	0.15 ± 0.06	0.19 ± 0.07
Caudate	0.06 ± 0.02	0.39 ± 0.05	0.06 ± 0.01	0.11 ± 0.06	0.20 ± 0.11
Thalamus	0.07 ± 0.02	0.43 ± 0.05	0.07 ± 0.01	0.03 ± 0.01	0.13 ± 0.06
Cerebellum (1TCM)	0.07 ± 0.02	0.41 ± 0.03	0.06 ± 0.01		

1TCM = 1-tissue-compartment model.
Values are mean ± SD.

TABLE 2. BP_{ND} Values Obtained by Different Methods and Scan Times

	Indirect kinetic method		SRTM method		Transient equilibrium method	
Region	90 min	60 min	90 min	60 min	BP_{ND}	Time (min)*
Putamen	0.82 ± 0.09	0.83 ± 0.09	0.78 ± 0.07	0.79 ± 0.08	0.76 ± 0.07	36.4 ± 4.5
Caudate	0.59 ± 0.11	0.59 ± 0.10	0.55 ± 0.09	0.56 ± 0.13	0.60 ± 0.09	39.6 ± 5.7
Thalamus	0.28 ± 0.06	0.28 ± 0.05	0.24 ± 0.04	0.31 ± 0.18	0.23 ± 0.05	29.2 ± 11.3

*Time of transient equilibrium (min).
Values are mean ± SD.

BP_{ND}. The error in BP_{ND} calculated by the transient equilibrium method was smallest when the K_1 value was 0.44, but BP_{ND} was overestimated when the K_1 value was lower than 0.36 and was underestimated when it was higher than 0.52 (Fig. 7). [Fig. 7]

DISCUSSION

Studies using agonist radioligands such as ^{11}C-PHNO to examine the high-affinity state of the dopamine D_2 receptor in the human brain have been reported previously (*32*). Our study describes the first, to our knowledge, PET examination using the agonist radioligand ^{11}C-MNPA to visualize binding to G-protein–coupled receptors in the human brain. After the intravenous injection of ^{11}C-MNPA, radioactivity appeared rapidly in the brain and was washed out in a fashion similar to that previously reported in nonhuman primates (*20*). Radioactivity was highest in the putamen and slightly lower in the caudate, moderate in the thalamus, and lowest in the cerebellum. This regional distribution is similar to that shown in nonhuman primates with ^{11}C-MNPA (*20,21*) and is in accordance with the known distribution of dopamine D_2 receptors, as demonstrated with antagonist radioligands such as ^{11}C-raclopride in the human brain (*33*). Finnema also reported blocking data with a dopamine D_2 antagonist in nonhuman primates (*20*). The pretreatment with raclopride, compared with the baseline condition, demonstrated high specific binding of the dopamine D_2 receptor by reducing the striatum-to-cerebellum ratio. The striatal BP_{ND} values of ^{11}C-MNPA were about one third of those in previous studies with the antagonist radioligand ^{11}C-raclopride (*33*). The K_d value of ^{11}C-raclopride in the human brain in vivo has been reported to be 9.1 nM (*34*), and the K_d value of ^{11}C-MNPA in the monkey brain in vivo has been reported to be 11.6 nM (*35*). Because the K_d values of ^{11}C-MNPA and ^{11}C-raclopride are similar in vitro, the difference in striatal BP_{ND} between ^{11}C-MNPA and ^{11}C-raclopride may reflect a difference in the density of available receptors (B_{max}) of the 2 radioligands. This interpretation is in line with the view that an agonist radioligand labels only the receptors in the high-affinity state, whereas an antagonist radioligand labels both high- and low-affinity-state dopamine D_2 receptors (*21,35*).

Ginovart et al. reported that ^{11}C-PHNO and ^{11}C-NPA in the cat were more sensitive to amphetamine-induced dopamine release than was ^{11}C-raclopride (*36*). The observation that ^{11}C-MNPA in nonhuman primates is also more sensitive to amphetamine-induced dopamine release than is ^{11}C-raclopride (*21*) has been taken as evidence for selective labeling of D_2 receptors in the high-affinity state. The relatively low BP_{ND} in the present study corroborates this view.

In this study, the indirect kinetic method with arterial blood sampling was used as the gold standard (*25*). Because arterial blood sampling is invasive, we examined the accuracy of the SRTM and transient equilibrium methods

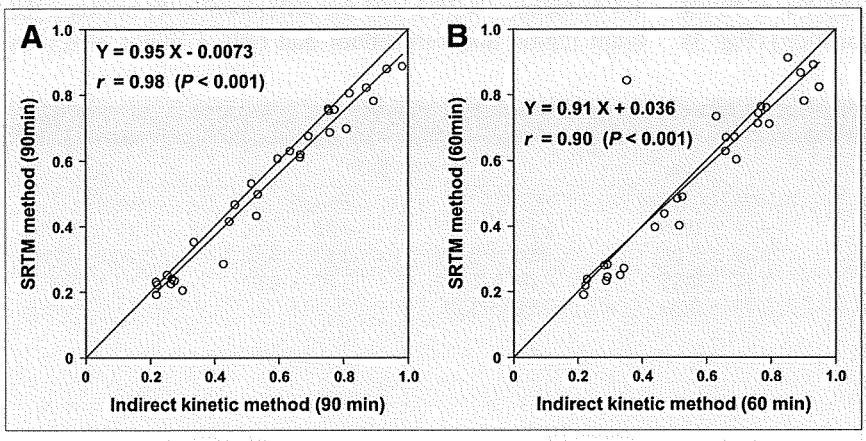

FIGURE 4. Comparison of BP_{ND} values in 3 regions (putamen, caudate, and thalamus) of 10 control subjects calculated by indirect kinetic and SRTM methods on the basis of data acquired over 90 (A) and 60 min (B).

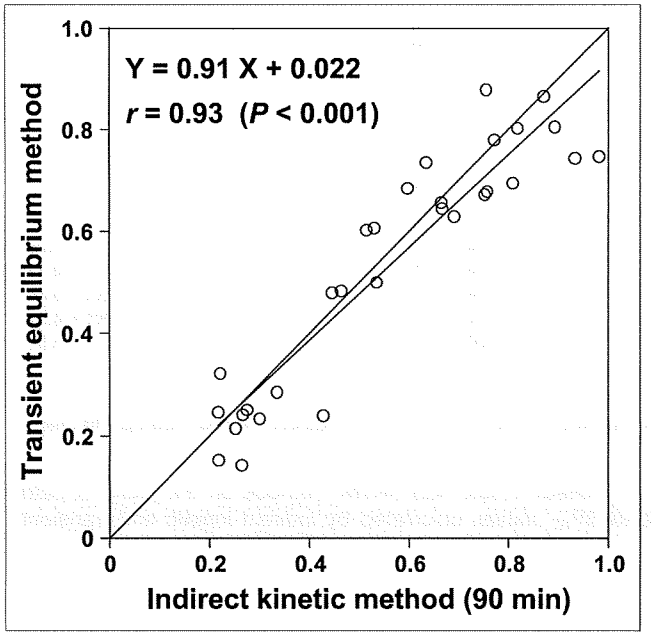

FIGURE 5. Comparison of BP_{ND} values in 3 regions (putamen, caudate, and thalamus) in 10 control subjects calculated by indirect kinetic and transient equilibrium methods.

for quantifying ^{11}C-MNPA binding using the cerebellum as the reference brain region. The SRTM and transient equilibrium methods had previously been validated for antagonist radioligands such as ^{11}C-raclopride and ^{11}C-FLB457 (*15,25,28*). In the present study, BP_{ND} of ^{11}C-MNPA obtained by the SRTM method was in good agreement with that obtained by the indirect kinetic method with data acquired for 60 and 90 min. The BP_{ND} value obtained by the transient equilibrium method was also in good agreement with the value obtained by the indirect kinetic method with data acquired for 90 min. Thus, it should be possible to use simplified protocols with no arterial blood sampling in applied clinical studies in humans.

In the simulation study, BP_{ND} calculated by the SRTM method was in good agreement with that calculated by the indirect kinetic method, although BP_{ND} was slightly overestimated. These results demonstrate the validity of the SRTM method for quantitating ^{11}C-MNPA binding also when blood flow and rate constants might be deviant. The present observation is in line with an ^{11}C-FLB457 study showing that the BP_{ND} value calculated by the SRTM method was not greatly affected by differences in K_1 between the brain regions and the cerebellum (*25*). Thus, the SRTM method is suitable for quantifying ^{11}C-MNPA binding when using a reference brain region without arterial blood sampling.

BP_{ND} calculated by the transient equilibrium method was not in good agreement with that calculated by the indirect kinetic method in the simulation study when the K_1 value in the brain region was small. The errors in BP_{ND} calculated by the transient equilibrium method were within the range of −15% to +15% when the K_1 value was 0.44 and 0.52 mL/cm^3/min, corresponding to 0.5–0.65 mL/cm^3/min of CBF. Although the transient equilibrium method might not be suitable for determining BP_{ND} in patients with low CBF, it is still a useful method for determining BP_{ND} without arterial blood sampling.

For clinical research, a short scanning time is preferred. In the present study, the BP_{ND} values calculated by the SRTM method with data acquired for 90 min were in good agreement with those obtained with data acquired for 60 min. In the simulation study, the BP_{ND} values obtained by the SRTM method with data acquired for 60 min were in good agreement with BP_{ND} values obtained by the indirect kinetic method, except with extremely low K_1. These results suggest that the SRTM method with data acquired for 60 min is valid for clinical studies in patients with neuropsychiatric disorders such as schizophrenia and depression.

CONCLUSION

The regional distribution of ^{11}C-MNPA was in good agreement with previous PET studies of dopamine D_2 receptors in the human brain using antagonist radioligands such as ^{11}C-raclopride and ^{11}C-FLB457. The BP_{ND} values

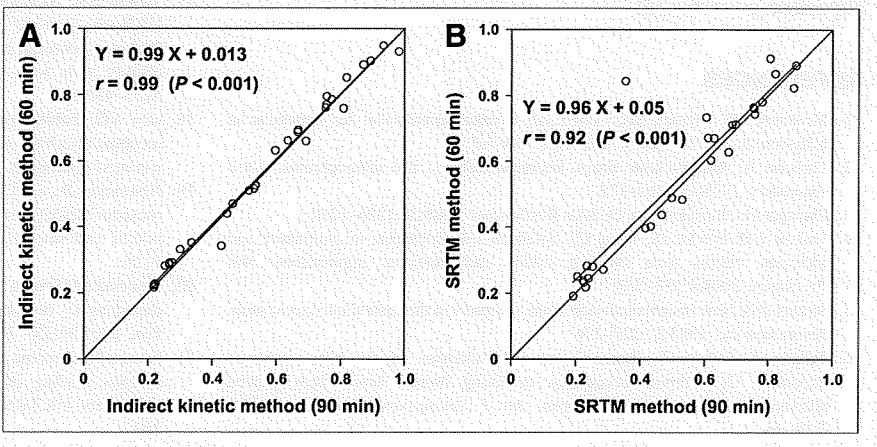

FIGURE 6. Comparison of BP_{ND} values in 3 regions (putamen, caudate, and thalamus) in 10 control subjects calculated by indirect kinetic (A) and SRTM (B) methods on the basis of data acquired over 90 and 60 min.

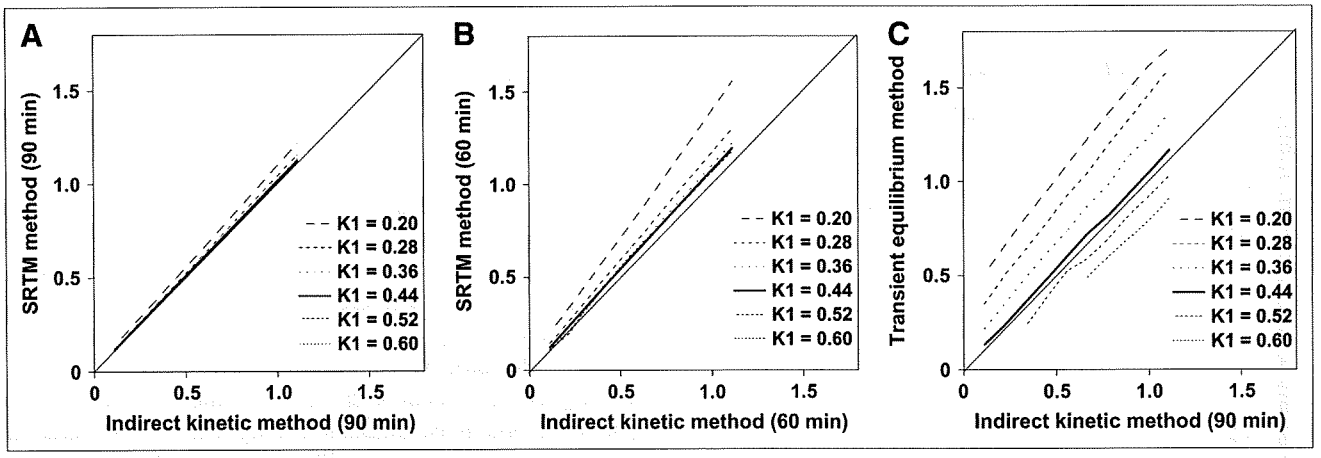

FIGURE 7. Comparison of simulated BP_{ND} values calculated by indirect kinetic and SRTM methods on the basis of data acquired over 90 (A) and 60 min (B). (C) Comparison of simulated BP_{ND} values calculated by indirect kinetic and transient equilibrium methods.

measured by the indirect kinetic model were in good agreement with those measured by the SRTM method with data acquired for 60 and 90 min. The BP_{ND} values measured by the transient equilibrium method also corresponded well with those measured by the indirect kinetic model with data acquired for 90 min. Simulation studies showed that errors in BP_{ND} measured by the SRTM method were small. The SRTM method with data acquired for 60 and 90 min is suitable for estimation of dopamine D_2 receptor bindings using ^{11}C-MNPA.

ACKNOWLEDGMENTS

We thank Katsuyuki Tanimoto, Takahiro Shiraishi, and Akira Ando for their assistance in performing the PET experiments at the National Institute of Radiological Sciences. We also thank Yoshiko Fukushima of the National Institute of Radiological Sciences for her help as clinical research coordinator. This study was supported by a consignment expense for the Molecular Imaging Program on "Research Base for PET Diagnosis" from the Ministry of Education, Culture, Sports, Science and Technology, Japanese government.

REFERENCES

1. Montague PR, Hyman SE, Cohen JD. Computational roles for dopamine in behavioural control. *Nature.* 2004;431:760–767.
2. Carlsson A. Antipsychotic drugs, neurotransmitters, and schizophrenia. *Am J Psychiatry.* 1978;135:165–173.
3. Ehringer H, Hornykiewicz O. *Klin Wochenschr.* 1960;38:1236–1239.
4. Volkow ND, Fowler JS, Wang GJ, Swanson JM. Dopamine in drug abuse and addiction: results from imaging studies and treatment implications. *Mol Psychiatry.* 2004;9:557–569.
5. Strange PG. New insights into dopamine receptors in the central nervous system. *Neurochem Int.* 1993;22:223–236.
6. Takano A, Suhara T, Ikoma Y, et al. Estimation of the time-course of dopamine D_2 receptor occupancy in living human brain from plasma pharmacokinetics of antipsychotics. *Int J Neuropsychopharmacol.* 2004; 7:19–26.
7. Yasuno F, Suhara T, Okubo Y, et al. Low dopamine D_2 receptor binding in subregions of the thalamus in schizophrenia. *Am J Psychiatry.* 2004;161:1016–1022.
8. Suhara T, Okubo Y, Yasuno F, et al. Decreased dopamine D_2 receptor binding in the anterior cingulate cortex in schizophrenia. *Arch Gen Psychiatry.* 2002;59: 25–30.
9. Yasuno F, Suhara T, Okubo Y, et al. Dose relationship of limbic-cortical D_2-dopamine receptor occupancy with risperidone. *Psychopharmacology (Berl).* 2001;154:112–114.
10. Talvik M, Nordstrom AL, Okubo Y, et al. Dopamine D_2 receptor binding in drug-naive patients with schizophrenia examined with [^{11}C]raclopride and positron emission tomography. *Psychiatry Res.* 2006;148:165–173.
11. Talvik M, Nordstrom AL, Olsson H, Halldin C, Farde L. Decreased thalamic D_2/D_3 receptor binding in drug-naive patients with schizophrenia: a PET study with [^{11}C]FLB 457. *Int J Neuropsychopharmacol.* 2003;6:361–370.
12. Sibley DR, De Lean A, Creese I. Anterior pituitary dopamine receptors: demonstration of interconvertible high and low affinity states of the D_2 dopamine receptor. *J Biol Chem.* 1982;257:6351–6361.
13. Halldin C, Gulyas B, Langer O, Farde L. Brain radioligands: state of the art and new trends. *Q J Nucl Med.* 2001;45:139–152.
14. Olsson H, Halldin C, Swahn CG, Farde L. Quantification of [^{11}C]FLB 457 binding to extrastriatal dopamine receptors in the human brain. *J Cereb Blood Flow Metab.* 1999;19:1164–1173.
15. Farde L, Eriksson L, Blomquist G, Halldin C. Kinetic analysis of central [^{11}C]raclopride binding to D_2-dopamine receptors studied by PET: a comparison to the equilibrium analysis. *J Cereb Blood Flow Metab.* 1989;9:696–708.
16. Hwang DR, Kegeles LS, Laruelle M. (-)-*N*-[^{11}C]propyl-norapomorphine: a positron-labeled dopamine agonist for PET imaging of D_2 receptors. *Nucl Med Biol.* 2000;27:533–539.
17. Wilson AA, McCormick P, Kapur S, et al. Radiosynthesis and evaluation of [^{11}C]-(+)-4-propyl-3,4,4a,5,6,10b-hexahydro-2H-naphtho[1,2-b][1,4]oxazin-9-ol as a potential radiotracer for in vivo imaging of the dopamine D_2 high-affinity state with positron emission tomography. *J Med Chem.* 2005;48: 4153–4160.
18. Gao YG, Baldessarini RJ, Kula NS, Neumeyer JL. Synthesis and dopamine receptor affinities of enantiomers of 2-substituted apomorphines and their *N*-n-propyl analogues. *J Med Chem.* 1990;33:1800–1805.
19. Neumeyer JL, Gao YG, Kula NS, Baldessarini RJ. Synthesis and dopamine receptor affinity of (*R*)-(-)-2-fluoro-*N*-n-propylnorapomorphine: a highly potent and selective dopamine D_2 agonist. *J Med Chem.* 1990;33:3122–3124.
20. Finnema SJ, Seneca N, Farde L, et al. A preliminary PET evaluation of the new dopamine D_2 receptor agonist [^{11}C]MNPA in cynomolgus monkey. *Nucl Med Biol.* 2005;32:353–360.
21. Seneca N, Finnema SJ, Farde L, et al. Effect of amphetamine on dopamine D_2 receptor binding in nonhuman primate brain: a comparison of the agonist radioligand [^{11}C]MNPA and antagonist [^{11}C]raclopride. *Synapse.* 2006;59:260–269.

22. Friston KJ, Frith CD, Liddle PF, Dolan RJ, Lammertsma AA, Frackowiak RS. The relationship between global and local changes in PET scans. *J Cereb Blood Flow Metab.* 1990;10:458–466.
23. Innis RB, Cunningham VJ, Delforge J, et al. Consensus nomenclature for in vivo imaging of reversibly binding radioligands. *J Cereb Blood Flow Metab.* 2007;27:1533–1539.
24. Martres MP, Bouthenet ML, Sales N, Sokoloff P, Schwartz JC. Widespread distribution of brain dopamine receptors evidenced with [^{125}I]iodosulpride, a highly selective ligand. *Science.* 1985;228:752–755.
25. Ito H, Sudo Y, Suhara T, Okubo Y, Halldin C, Farde L. Error analysis for quantification of [^{11}C]FLB 457 binding to extrastriatal D_2 dopamine receptors in the human brain. *Neuroimage.* 2001;13:531–539.
26. Ito H, Ota M, Ikoma Y, et al. Quantitative analysis of dopamine synthesis in human brain using positron emission tomography with L-[beta-^{11}C]DOPA. *Nucl Med Commun.* 2006;27:723–731.
27. Lammertsma AA, Hume SP. Simplified reference tissue model for PET receptor studies. *Neuroimage.* 1996;4:153–158.
28. Ito H, Hietala J, Blomqvist G, Halldin C, Farde L. Comparison of the transient equilibrium and continuous infusion method for quantitative PET analysis of [^{11}C]raclopride binding. *J Cereb Blood Flow Metab.* 1998;18:941–950.
29. Hatazawa J, Fujita H, Kanno I, et al. Regional cerebral blood flow, blood volume, oxygen extraction fraction, and oxygen utilization rate in normal volunteers measured by the autoradiographic technique and the single breath inhalation method. *Ann Nucl Med.* 1995;9:15–21.
30. Renkin EM. Transport of potassium-42 from blood to tissue in isolated mammalian skeletal muscles. *Am J Physiol.* 1959;197:1205–1210.
31. Crone C. The permeability of capillaries in various organs as determined by use of the 'indicator diffusion' method. *Acta Physiol Scand.* 1963;58:292–305.
32. Willeit M, Ginovart N, Kapur S, et al. High-affinity states of human brain dopamine $D_{2/3}$ receptors imaged by the agonist [^{11}C]-(+)-PHNO. *Biol Psychiatry.* 2006;59:389–394.
33. Ito H, Takahashi H, Arakawa R, Takano H, Suhara T. Normal database of dopaminergic neurotransmission system in human brain measured by positron emission tomography. *Neuroimage.* 2008;39:555–565.
34. Farde L, Hall H, Pauli S, Halldin C. Variability in D_2-dopamine receptor density and affinity: a PET study with [^{11}C]raclopride in man. *Synapse.* 1995;20:200–208.
35. Finnema SJ, Seneca N, Farde L, et al. Scatchard analysis of the D_2 receptor agonist [^{11}C]MNPA in the monkey brain using PET [abstract]. *Eur J Nucl Med Mol Imaging.* 2005;32(S82):293.
36. Ginovart N, Galineau L, Willeit M, et al. Binding characteristics and sensitivity to endogenous dopamine of [^{11}C]-(+)-PHNO, a new agonist radiotracer for imaging the high-affinity state of D_2 receptors in vivo using positron emission tomography. *J Neurochem.* 2006;97:1089–1103.

Journal of Psychiatric Research 43 (2009) 1219–1223

Contents lists available at ScienceDirect

Journal of Psychiatric Research

journal homepage: www.elsevier.com/locate/jpsychires

Increase in thalamic binding of [^{11}C]PE2I in patients with schizophrenia: A positron emission tomography study of dopamine transporter

Ryosuke Arakawa [a,b], Tetsuya Ichimiya [a,b], Hiroshi Ito [a], Akihiro Takano [a], Masaki Okumura [a,b], Hidehiko Takahashi [a], Harumasa Takano [a], Fumihiko Yasuno [a], Motoichiro Kato [c], Yoshiro Okubo [b], Tetsuya Suhara [a,*]

[a] Molecular Neuroimaging Group, Molecular Imaging Center, National Institute of Radiological Sciences, 4-9-1, Anagawa, Inage-ku, Chiba 263-8555, Japan
[b] Department of Neuropsychiatry, Nippon Medical School, Tokyo, Japan
[c] Department of Neuropsychiatry, Keio University School of Medicine, Tokyo, Japan

ARTICLE INFO

Article history:
Received 15 January 2009
Received in revised form 5 March 2009
Accepted 21 April 2009

Keywords:
Dopamine transporter
Schizophrenia
Thalamus
Positron emission tomography
[^{11}C]PE2I
PANSS

ABSTRACT

Previous *in vivo* imaging studies reported no difference in dopamine transporter (DAT) bindings in the striatum between control subjects and patients with schizophrenia. However, as the signals of radioligands with moderate affinity were insufficient for allowing the evaluation of small amounts of DAT, DAT binding in extrastriatal regions has not been determined. Positron emission tomography scanning using [^{11}C]PE2I was performed on eight patients with schizophrenia and twelve normal control subjects. Binding potential (BP_{ND}) for DAT in the caudate, putamen, thalamus and substantia nigra was calculated, using the cerebellum as reference region. In patients with schizophrenia, clinical symptoms were evaluated by Positive and Negative Syndrome Scale (PANSS). BP_{ND} in the thalamus of patients with schizophrenia was significantly higher than in control subjects ($P = 0.044$). In patients with schizophrenia, there were significantly positive correlations between BP_{ND} in the thalamus and total ($r = 0.75$), positive ($r = 0.78$) and negative PANSS scores ($r = 0.82$). Altered DAT in the thalamus might be related to the pathophysiology and clinical symptoms of schizophrenia.

1. Introduction

One of the most accepted hypotheses concerning the pathophysiology of schizophrenia are the hyperactivity of dopaminergic neurotransmission. This 'dopamine hypothesis' is supported by the facts that antipsychotic effects are mainly related to dopamine D_2 receptor antagonism and that dopamine stimulating agents can cause psychotic symptoms such as hallucination or delusion. Dopamine transporter (DAT) plays a role in the reuptake of dopamine into pre-synaptic nerves and regulates dopaminergic transmission in the synaptic cleft. DAT inhibitors such as cocaine increase dopamine concentration in the synaptic cleft (Schlaepfer et al., 1997) and worsen the clinical course of schizophrenia, e.g., exacerbating positive and negative symptoms, increasing the risk of relapse, or hospitalization (Green, 2005).

Previous *in vivo* imaging studies using positron emission tomography (PET) or single photon emission computed tomography (SPECT) reported no difference in DAT bindings between control subjects and patients with schizophrenia (Hsiao et al., 2003; Laakso et al., 2000; Laruelle et al., 2000; Lavalaye et al., 2001; Schmitt et al., 2005, 2006, 2008; Yang et al., 2004) except for one study reporting lower binding in patients with schizophrenia as compared with controls (Mateos et al., 2007). However, those studies evaluated DAT binding only in the striatum, as DAT density in extrastriatal regions is very low (in a postmortem human study, [^{125}I]PE2I binding in the thalamus was reported to be 15% of that in the striatum and negligible in the cortex) (Hall et al., 1999). The recent development of [^{11}C]PE2I, which has high affinity ($K_i = 17$ nM) and selectivity (more than 30-fold for other monoamine transporters) for DAT, allows the evaluation of extrastiatal DAT bindings (Halldin et al., 2003; Hirvonen et al., 2008; Jucaite et al., 2006). In this study, we evaluated DAT binding in the striatal and extrastriatal regions of patients with schizophrenia using [^{11}C]PE2I.

2. Materials and methods

2.1. Subjects

Eight patients (age range 25–52 yr, mean ± SD: 36.5 ± 9.5 yr) diagnosed with schizophrenia or schizophreniform disorder according to DSM-IV criteria participated in this study. Four patients with schizophreniform disorder met the criteria for schizophrenia at six month follow-up. Exclusion criteria were current

* Corresponding author. Tel.: +81 43 206 3251; fax: +81 43 253 0396.
E-mail address: suhara@nirs.go.jp (T. Suhara).

0022-3956/$ - see front matter © 2009 Elsevier Ltd. All rights reserved.
doi:10.1016/j.jpsychires.2009.04.009

Table 1
Demographic and clinical characteristics.

	Controls	Patients
N	12	8
Age (years)	33.2 ± 12.0	36.5 ± 9.5
Gender (M/F)	10/2	6/2
Naïve/free		6/2
Duration of illness (months)		32.1 ± 42.8
PANSS (total)		77.8 ± 18.8
Positive		17.8 ± 4.8
Negative		18.9 ± 6.5
General		41.1 ± 10.8

Values are mean ± SD.

or past substance abuse, organic brain disease, or epilepsy. Demographic and clinical data are shown in Table 1. Six of the patients were antipsychotic naïve and two had been antipsychotic-free for at least six months before the PET scan. Three patients had taken benzodiazepines the night before the PET scan.

Psychopathological symptoms were assessed by three experienced psychiatrists on the same day as the PET scans using the Positive and Negative Syndrome Scale (PANSS), and consensus ratings were used. PANSS scores used were total score and subscores for positive symptom, negative symptom and general symptom.

Twelve normal control subjects (age range 23–56 yr, mean ± SD: 33.2 ± 12.0 yr) also participated. None of them had a history of psychiatric or neurological disorders, brain injury, chronic somatic illness, or substance abuse. None had taken any drugs within two weeks before the PET scan.

After complete description of this study, written informed consent was obtained from all subjects. The study was approved by the Ethics and Radiation Safety Committee of the National Institute of Radiological Sciences, Chiba, Japan. Data were collected from 4/2003 to 8/2006.

2.2. PET procedure

A PET scanner system, ECAT EXACT HR+(CTI-Siemens, Knoxville, TN, USA), was used for all measurements. A head fixation device was used to minimize head movement. A transmission scan for attenuation correction was performed using a ^{68}Ge–^{68}Ga source before each scan. A dynamic PET scan was performed for 90 min (20 s × 9, 1 min × 5, 2 min × 4, 4 min × 11, 5 min × 6) after intravenous bolus injection of 214.7 ± 13.7 MBq (mean ± SD) of [^{11}C]PE2I. The specific radioactivity of [^{11}C]PE2I was 344.5 ± 355.3 MBq/nmol. Injected dose and specific radioactivity between the control and patient groups were not significantly different (two-tailed *t*-test; $P = 0.15$ and $P = 0.16$, respectively). Since two previous quantitative studies of [^{11}C]PE2I had reported good reliability with scan times of 63 and 69 min, the scan time of 90 min was considered sufficient for estimation of DAT bindings especially in extrastriatal regions (Hirvonen et al., 2008; Jucaite et al., 2006). Magnetic resonance (MR) images of the brain were acquired with a 1.5 Tesla MR imaging system, Gyroscan NT (Philips Medical Systems, Best, Netherlands). T1-weighted images were obtained at 1 mm slices. All subjects were free of organic brain lesions.

2.3. Data analysis

All MR images were coregistered to the PET images using the statistical parametric mapping (SPM2) system. MR images were transformed into the standard brain size and shape by SPM2 (anatomic standardization). All PET images were also transformed into the standard brain size and shape using the same parameters as the MR image standardization. Thus, brain images of all subjects had the same anatomic format (Ito et al., 2008). Motion corrections were not made.

Regions of interest (ROIs) were drawn on all anatomically standardized PET images with reference to the T1-weighted MR images. ROIs were defined for the cerebellar cortex, caudate head, putamen, substantia nigra and thalamus (Fig. 1).

Binding potential (BP_{ND}) was calculated by the simplified reference tissue model (SRTM) method. The cerebellum was used as reference region because of its negligible density of DAT (Hall et al., 1999). In this study, the software package PMOD (PMOD Technologies, Zurich, Switzerland) was used to calculate BP_{ND}.

2.4. Statistics

Statistical analysis concerning the difference of BP_{ND} for each ROI between patients and controls was performed by two-tailed *t*-test. Correlations between BP_{ND} of patients with schizophrenia and age, duration of illness, and PANSS scores were evaluated using Pearson's correlation coefficient. In all analyses, $P < 0.05$ was considered significant.

3. Results

The BP_{ND} values of control subjects and patients with schizophrenia are shown in Table 2. The BP_{ND} value in the thalamus was significant higher in patients with schizophrenia than in con-

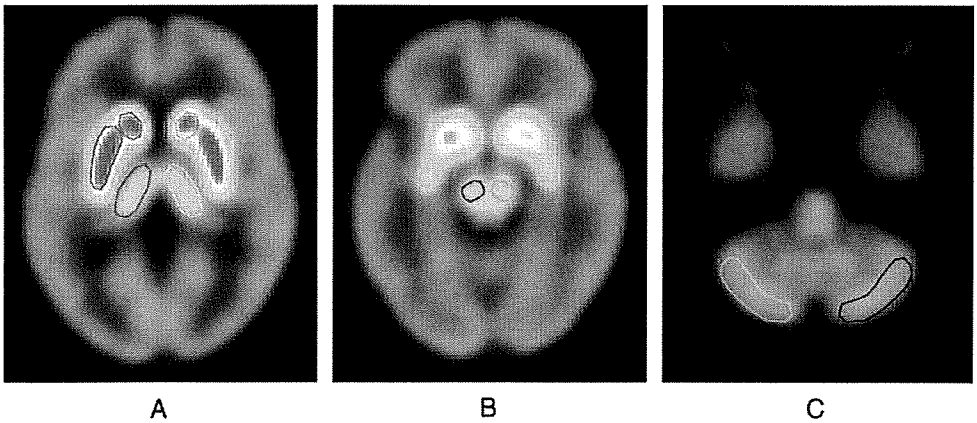

Fig. 1. Summated images of [^{11}C]PE2I with regions of interest. Average normalized images of twelve control subjects are shown at the level of caudate, putamen and thalamus (A), substantia nigra (B) and cerebellum (C).

Table 2
BP_{ND} in all regions.

	BP_{ND}[a]				*t*-test	
Region	Controls	Patients	% Change[b]	Effect size	*t*	*P*
Caudate	7.54 ± 1.22	8.21 ± 1.38	8.9 ± 18.4 (−6.5–24.2)%	0.55	1.14	0.27
Putamen	7.54 ± 1.25	8.23 ± 0.71	9.2 ± 9.4 (1.3–17.0)%	0.55	1.41	0.18
Thalamus	0.28 ± 0.08	0.36 ± 0.07	27.9 ± 25.8 (6.3–49.5)%	1.0	2.16	0.044*
Substantia nigra	1.09 ± 0.16	1.13 ± 0.12	4.1 ± 11.3 (−5.3–13.6)%	0.25	0.66	0.52

[a] Values are mean ± SD.
[b] Values are mean ± SD and 95% confidence interval.
* $P < 0.05$.

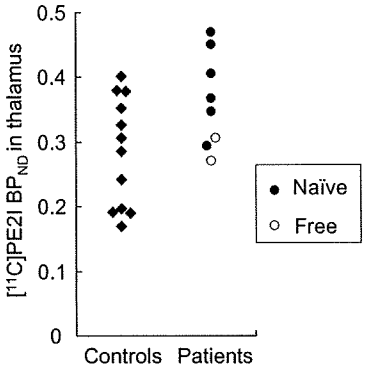

Fig. 2. BP_{ND} in the thalamus of normal controls and patients with schizophrenia. BP_{ND} of patients with schizophrenia was significantly higher than that of the control group (df = 18, $t = 2.16$, $P = 0.044$).

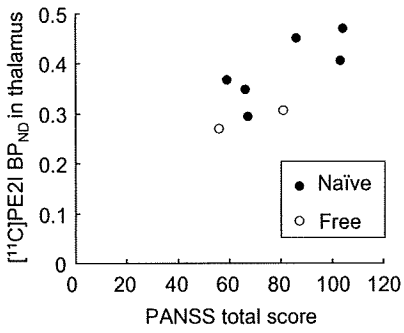

Fig. 3. Relationship between BP_{ND} in the thalamus of patients with schizophrenia and total PANSS score. There were significantly positive correlations between BP_{ND} and total PANSS score ($r = 0.75$, $P = 0.032$).

trols (df = 18, $t = 2.16$, $P = 0.044$) (Table 2, Fig. 2). There were no significant differences in BP_{ND} between the two groups in the caudate, putamen or substantia nigra. In patients with schizophrenia, there were significant positive correlations between BP_{ND} in the thalamus and total PANSS score ($r = 0.75$, $P = 0.032$), positive ($r = 0.78$, $P = 0.023$) and negative PANSS scores ($r = 0.82$, $P = 0.014$), but no correlation was observed with the general PANSS score (Table 3, Fig. 3). There was no significant correlation between BP_{ND} in other regions and clinical symptoms. There was also no significant correlation between BP_{ND} in each region and age or duration of illness.

4. Discussion

The *in vivo* evaluation of thalamic DAT had not been previously performed in detail due to its very low density as compared to that in the striatum (Hall et al., 1999). [^{11}C]PE2I allows the estimation of specific binding in low density regions because of its high affinity and selectivity for DAT (Halldin et al., 2003; Hirvonen et al., 2008; Jucaite et al., 2006). In this study, BP_{ND} in the thalamus of patients with schizophrenia was significantly higher than that of control subjects and was positively correlated with clinical symptoms. There was no significant difference in the area under the time activity curves of the cerebellum between controls and the patient group (two-tailed *t*-test; $P = 0.37$), suggesting that the higher DAT bindings were not due to cerebellar difference. An effect of endogenous dopamine on [^{11}C]PE2I binding has not been reported. However, as [^{11}C]PE2I is a high-affinity radioligand ($K_i = 17$ nM), it is reasonable to expect such an effect based on the result from a high-affinity ralioligand for serotonin transporter, [^{11}C]DASB ($K_i = 1.1$ nM) (Wilson et al., 2000). [^{11}C]DASB binding did not change by manipulation of endogenous serotonin in human brain (Praschak-Rieder et al., 2005; Talbot et al., 2005). Although these results may not apply directly to [^{11}C]PE2I binding, high [^{11}C]PE2I binding can nevertheless be interpreted as high DAT density.

The thalamus has been considered as the key brain structure of processing or integrating sensory information related to emotional or cognitive functions (Clinton and Meador-Woodruff, 2004). Several studies have reported morphological abnormalities of the thalamus in patients with schizophrenia using MR imaging or postmortem studies (Clinton and Meador-Woodruff, 2004). Regarding dopaminergic transmission, increased dopamine concentrations in the thalamus of patients with schizophrenia were reported in a postmortem study (Oke and Adams, 1987). The distribution of dopaminergic innervation in the thalamus was reported recently using immunohistochemistry in monkey (Melchitzky and Lewis, 2001) and human brain (Garcia-Cabezas et al., 2007). These studies reported that thalamic dopamine or DAT was relatively higher in the midline and mediodorsal nuclei. In patients

Table 3
Correlation between regional BP_{ND} and PANSS scores.

	Total		Positive		Negative		General	
Region	*r*	*P*	*r*	*P*	*r*	*P*	*r*	*P*
Caudate	−0.04	0.93	0.03	0.95	0.10	0.81	−0.14	0.74
Putamen	−0.44	0.28	−0.42	0.31	−0.03	0.93	−0.55	0.15
Thalamus	0.75	0.032*	0.78	0.023*	0.82	0.014*	0.47	0.24
Substantia nigra	0.04	0.93	0.26	0.53	0.03	0.94	−0.07	0.86

* $P < 0.05$.

with schizophrenia, lower dopamine D_2 receptor binding was observed in the thalamus using PET with [^{11}C]FLB457 (Buchsbaum et al., 2006; Talvik et al., 2003; Yasuno et al., 2004) and [^{11}C]raclopride (Talvik et al., 2006). Significant differences in calcyon and spinophilin, dopamine receptor-associated intracellular proteins, and no difference in vesicular monoamine transporter (VMAT) binding of the thalamus were reported in a postmortem study of patients with schizophrenia and controls (Clinton et al., 2005). Assuming that low dopamine D_2 receptor binding is related to the disruption of the feedback system of dopamine release mediated by GABA interneuron (Takahashi et al., 2006), a high turnover of dopamine at the synapse would exist as a hyper-dopaminergic state. Although the function of DAT in the thalamus has remained unclear, high DAT bindings may suggest a hyper-dopaminergic state of pre-synaptic dopamine function in patients with schizophrenia.

Most of the previous PET and SPECT studies reported that DAT binding in the striatum did not differ between subjects and patients with schizophrenia (Hsiao et al., 2003; Laakso et al., 2000; Laruelle et al., 2000; Lavalaye et al., 2001; Schmitt et al., 2005, 2006, 2008; Yang et al., 2004), and our present results were in line with these reports. DAT binding in the substantia nigra also showed no difference between control subjects and patients with schizophrenia. However, BP_{ND} in the striatum using SRTM can be underestimated as compared to the values by kinetic model analyses with arterial blood sampling (Hirvonen et al., 2008; Jucaite et al., 2006). This might affect the results in the striatum.

In this study, the number of subjects was small, and in the statistical analysis we did not perform multiple comparisons regarding group differences of BP_{ND} between patients and controls to avoid type II error. Moreover, two of the eight patients were in a drug-free state, not drug-naïve state. Nonetheless, even when the two drug-free patients were excluded, the group difference of BP_{ND} in the thalamus was still observed (two-tailed t-test; $P = 0.018$). Further study with larger numbers of subjects in a drug-naïve state will be needed.

In conclusion, [^{11}C]PE2I binding in the thalamus of patients with schizophrenia was significantly higher than in control subjects and was correlated with clinical symptoms. Altered DAT in the thalamus might be related to the pathophysiology and clinical symptoms of schizophrenia.

Conflict of interest

All authors have no conflicts of interest.

Contributors

R. Arakawa, T. Ichimiya, A. Takano, F. Yasuno, and T. Suhara designed the study and wrote the protocol. R. Arakawa, T. Ichimiya, A. Takano, M. Okumura, H. Takahashi, H. Takano, F. Yasuno, M. Kato, and Y. Okubo recruited the patients and made psychiatric evaluations. R. Arakawa, H. Ito, M. Okumura, H. Takahashi, and H. Takano participated in the data analysis. R. Arakawa wrote the first draft of the manuscript. R. Arakawa, H. Ito, H. Takahashi, H. Takano, M. Kato, Y. Okubo, and T. Suhara had discussions and corrected the manuscript. All authors contributed to and have approved the final manuscript.

Role of funding source

This study was supported by a consignment expense for the Molecular Imaging Program on "Research Base for PET Diagnosis" from the Ministry of Education, Culture, Sports, Science and Technology (MEXT), Japanese Government. The sponsors of the study had no role in the study design, collection, analysis, and interpretation of data, in the writing of the report, or in the decision to submit the paper for publication.

Acknowledgements

We thank Mr. Katsuyuki Tanimoto, Mr. Takahiro Shiraishi, Mr. Akira Ando and Mr. Toshio Miyamoto for their assistance in performing the PET experiments, and Ms. Yoshiko Fukushima for her help as clinical research coordinator at the National Institute of Radiological Sciences.

References

Buchsbaum MS, Christian BT, Lehrer DS, Narayanan TK, Shi B, Mantil J, et al. D2/D3 dopamine receptor binding with [F-18]fallypride in thalamus and cortex of patients with schizophrenia. Schizophrenia Research 2006;85:232–44.

Clinton SM, Meador-Woodruff JH. Thalamic dysfunction in schizophrenia: neurochemical, neuropathological, and in vivo imaging abnormalities. Schizophrenia Research 2004;69:237–53.

Clinton SM, Ibrahim HM, Frey KA, Davis KL, Haroutunian V, Meador-Woodruff JH. Dopaminergic abnormalities in select thalamic nuclei in schizophrenia: involvement of the intracellular signal integrating proteins calcyon and spinophilin. The American Journal of Psychiatry 2005;162:1859–71.

Garcia-Cabezas MA, Rico B, Sanchez-Gonzalez MA, Cavada C. Distribution of the dopamine innervation in the macaque and human thalamus. NeuroImage 2007;34:965–84.

Green AI. Schizophrenia and comorbid substance use disorder: effects of antipsychotics. The Journal of Clinical Psychiatry 2005;66(Suppl. 6):21–6.

Hall H, Halldin C, Guilloteau D, Chalon S, Emond P, Besnard J, et al. Visualization of the dopamine transporter in the human brain postmortem with the new selective ligand [125I]PE2I. NeuroImage 1999;9:108–16.

Halldin C, Erixon-Lindroth N, Pauli S, Chou YH, Okubo Y, Karlsson P, et al. [11C]PE2I: a highly selective radioligand for PET examination of the dopamine transporter in monkey and human brain. European Journal of Nuclear Medicine and Molecular Imaging 2003;30:1220–30.

Hirvonen J, Johansson J, Teras M, Oikonen V, Lumme V, Virsu P, et al. Measurement of striatal and extrastriatal dopamine transporter binding with high-resolution PET and [11C]PE2I: quantitative modeling and test-retest reproducibility. Journal of Cerebral Blood Flow and Metabolism 2008;28:1059–69.

Hsiao MC, Lin KJ, Liu CY, Tzen KY, Yen TC. Dopamine transporter change in drug-naive schizophrenia: an imaging study with 99mTc-TRODAT-1. Schizophrenia Research 2003;65:39–46.

Ito H, Takahashi H, Arakawa R, Takano H, Suhara T. Normal database of dopaminergic neurotransmission system in human brain measured by positron emission tomography. NeuroImage 2008;39:555–65.

Jucaite A, Odano I, Olsson H, Pauli S, Halldin C, Farde L. Quantitative analyses of regional [11C]PE2I binding to the dopamine transporter in the human brain: a PET study. European Journal of Nuclear Medicine and Molecular Imaging 2006;33:657–68.

Laakso A, Vilkman H, Alakare B, Haaparanta M, Bergman J, Solin O, et al. Striatal dopamine transporter binding in neuroleptic-naive patients with schizophrenia studied with positron emission tomography. The American Journal of Psychiatry 2000;157:269–71.

Laruelle M, Abi-Dargham A, van Dyck C, Gil R, D'Souza DC, Krystal J, et al. Dopamine and serotonin transporters in patients with schizophrenia: an imaging study with [123I]beta-CIT. Biological Psychiatry 2000;47:371–9.

Lavalaye J, Linszen DH, Booij J, Dingemans PM, Reneman L, Habraken JB, et al. Dopamine transporter density in young patients with schizophrenia assessed with [123I]FP-CIT SPECT. Schizophrenia Research 2001;47:59–67.

Mateos JJ, Lomena F, Parellada E, Mireia F, Fernandez-Egea E, Pavia J, et al. Lower striatal dopamine transporter binding in neuroleptic-naive schizophrenic patients is not related to antipsychotic treatment but it suggests an illness trait. Psychopharmacology 2007;191:805–11.

Melchitzky DS, Lewis DA. Dopamine transporter-immunoreactive axons in the mediodorsal thalamic nucleus of the macaque monkey. Neuroscience 2001;103:1033–42.

Oke AF, Adams RN. Elevated thalamic dopamine: possible link to sensory dysfunctions in schizophrenia. Schizophrenia Bulletin 1987;13:589–604.

Praschak-Rieder N, Wilson AA, Hussey D, Carella A, Wei C, Ginovart N, et al. Effects of tryptophan depletion on the serotonin transporter in healthy humans. Biological Psychiatry 2005;58:825–30.

Schlaepfer TE, Pearlson GD, Wong DF, Marenco S, Dannals RF. PET study of competition between intravenous cocaine and [11C]raclopride at dopamine receptors in human subjects. The American Journal of Psychiatry 1997;154:1209–13.

Schmitt GJ, Meisenzahl EM, Frodl T, La Fougere C, Hahn K, Moller HJ, et al. The striatal dopamine transporter in first-episode, drug-naive schizophrenic patients: evaluation by the new SPECT-ligand[99mTc]TRODAT-1. Journal of Psychopharmacology 2005;19:488–93.

Schmitt GJ, Frodl T, Dresel S, la Fougere C, Bottlender R, Koutsouleris N, et al. Striatal dopamine transporter availability is associated with the productive psychotic state in first episode, drug-naive schizophrenic patients. European Archives of Psychiatry and Clinical Neuroscience 2006;256:115–21.

Schmitt GJ, la Fougere C, Dresel S, Frodl T, Hahn K, Moller HJ, et al. Dual-isotope SPECT imaging of striatal dopamine: first episode, drug naive schizophrenic patients. Schizophrenia Research 2008;101:133–41.

Takahashi H, Higuchi M, Suhara T. The role of extrastriatal dopamine D2 receptors in schizophrenia. Biological Psychiatry 2006;59:919–28.

Talbot PS, Frankle WG, Hwang DR, Huang Y, Suckow RF, Slifstein M, et al. Effects of reduced endogenous 5-HT on the in vivo binding of the serotonin transporter radioligand 11C-DASB in healthy humans. Synapse 2005;55:164–75.

Talvik M, Nordstrom AL, Olsson H, Halldin C, Farde L. Decreased thalamic D2/D3 receptor binding in drug-naive patients with schizophrenia: a PET study with [11C]FLB 457. The International Journal of Neuropsychopharmacology 2003;6:361–70.

Talvik M, Nordstrom AL, Okubo Y, Olsson H, Borg J, Halldin C, et al. Dopamine D2 receptor binding in drug-naive patients with schizophrenia examined with raclopride-C11 and positron emission tomography. Psychiatry Research 2006;148:165–73.

Wilson AA, Ginovart N, Schmidt M, Meyer JH, Threlkeld PG, Houle S. Novel radiotracers for imaging the serotonin transporter by positron emission tomography: synthesis, radiosynthesis, and in vitro and ex vivo evaluation of 11C-labeled 2-(phenylthio)araalkylamines. Journal of Medicinal Chemistry 2000;43:3103–10.

Yang YK, Yu L, Yeh TL, Chiu NT, Chen PS, Lee IH. Associated alterations of striatal dopamine D2/D3 receptor and transporter binding in drug-naive patients with schizophrenia: a dual-isotope SPECT study. The American Journal of Psychiatry 2004;161:1496–8.

Yasuno F, Suhara T, Okubo Y, Sudo Y, Inoue M, Ichimiya T, et al. Low dopamine d2 receptor binding in subregions of the thalamus in schizophrenia. The American Journal of Psychiatry 2004;161:1016–22.